Received: 24 November 2021 | Revised: 28 January 2022 | Accepted: 3 February 2022

DOI: 10.1111/dgd.12777

RESEARCH ARTICLE

Development, Growth & Differentiation WILEY

Discrete embryonic character variation uncovers hidden ecological adaptations in lacertid lizards

Xenia Schlindwein[1,2] | Oleksandr Yaryhin[3] | Ingmar Werneburg[1,2]

[1]Fachbereich Geowissenschaften an der Universität Tübingen, Tübingen, Germany

[2]Senckenberg Centre for Human Evolution and Palaeoenvironment an der Universität Tübingen, Tübingen, Germany

[3]I.I. Schmalhausen Institute of Zoology of National Academy of Sciences of Ukraine, Kyiv, Ukraine

Correspondence
Ingmar Werneburg, Fachbereich Geowissenschaften an der Universität Tübingen, Hölderlinstraße 12, 72074 Tübingen, Germany.
Email: ingmar.werneburg@senckenberg.de

Funding information
Deutsche Forschungsgemeinschaft, Grant/Award Numbers: WE 5440/5-1, WE 5440/6-1

Communicating Editor: Tatsuya Hirasawa

Abstract

Embryogenesis is the first step in the ontogenetic life journey of any individual, and is thus a starting point for natural selection to cause evolutionary change. There are slight variations in the timing of embryonic development, known as heterochrony, which may eventually lead to major differences in adult anatomy. To test this hypothesis, the embryonic development of three closely related lizard species, *Darevskia armeniaca*, *Lacerta agilis*, and *L. viridis*, which are adapted to different habitats, was compared by analyzing discrete timing characters. Both intra- and interspecific variation was detected. The latter may be interpreted as embryonic pre-adaptions to later adult lifestyles, demonstrating that developmental penetrance manifests within a few million years. Traits with large intraspecific temporal variation, such as limb-related features, were susceptible to natural selection. In particular, the mountain-dwelling, climbing species *D. armeniaca* showed embryonic preadaptions by an early developing limb anlagen. This observation demonstrated interspecific variation, which was elusive in a previous comparative study based on purely metric data of developing limb lengths, and highlighted the importance of multiple data sources to draw robust conclusions about evolutionary change. Timing differences indicated unexplored ecological adaptations of the poorly understood lifestyle of these lizards. Thus, embryonic research provides a platform to explore superficially hidden evolutionary adaptations of all organisms on Earth.

KEYWORDS
developmental penetrance, embryogenesis, natural selection, organ development, reptiles, standard event system (SES)

1 | INTRODUCTION

Natural selection occurs not only in adults, but also throughout the ontogeny of every organism (Maier, 1999). For example, hatchlings of the European green lizard have an extraordinarily low chance of survival in their first year; their mortality rate increases up to 100% in years with bad conditions, while adults may live up to approximately ten years (Hill & Klepsch, 2008). One major source for selection is anatomical variation (Raff, 1996), resulting in major taxon diversification, as well as in fast radiation in lower taxonomic levels, such as 'families' or 'genera'. As individual anatomic features form during embryonic development, it is important to examine these for a comprehensive understanding of how evolutionary processes are linked to individual ontogeny. Werneburg et al. (2015) have argued that, in general, "the earlier an element appears during development, the more prominent it becomes in the adult because it has more time to grow and differentiate." Thus, the later a structure emerges, the smaller or less complex it will appear. Such adaptive heterochrony implies, among other things, deep developmental penetrance, indicating that evolutionary adaptations are genetically integrated into embryonic development (Hamrick, 2001; Richardson, 1999). In this way, morphological features that are

characteristic for adaptation in adults develop early and may become fully established should they be required directly after birth or hatching (Bickelmann et al., 2012).

A good model for these research questions are the true lizards, Lacertidae (Figure 1), which currently number over 300 species that "successfully radiated into a wide array of habitats and climate regions from subarctic tundra over temperate heath lands and forests, alpine meadows and Mediterranean maquis, steppe and gravel semi-deserts, and monsoonal rainforest to sandy dune systems in the desert" (Baeckens et al., 2015). This occurred in a relatively short time, geologically speaking, of approximately 85 million years (Kumar et al., 2017). To mirror this diversity, the intra- and interspecific differences in the ontogeny of three lacertid species adapted to different habitats was investigated: the Armenian rock lizard *Darevskia armeniaca*, sand lizard *Lacerta agilis*, and European green lizard *L. viridis*.

In a recent attempt to understand interspecific limb variation through the ontogeny of the three lacertid species, no significant difference among embryos, but only post-embryonic development of selected limb proportions was identified (Cordero et al., 2021). However, only selected metric traits were used in this approach, which did not account for internal anatomical specifications or differences in the general embryonic anatomy among the three species. The different nature of the data used in the present study may be better suited to distinguish changes in embryonic development.

Because development is a continuous process and traditional "normal embryonic staging" is not well suited for documenting variation (Richardson, 2022), the Standard Event System (SES) approach introduced by Werneburg (2009) was used, which uses discrete characters (Figure 2) to describe and compare intra- and interspecific differences in embryogenesis.

FIGURE 1 Embryos of different developmental periods and adults of the three species analyzed in this study. Photo of adult *Darevskia armeniaca*: Köhler, Babette (2019-08-11), via https://www.inaturalist.org/photos/47933393, CC BY-NC 4.0, accessed: 2022-04-11. Photo of adult *Lacerta agilis*: Böhringer, Friedrich (2007-08-30), via https://commons.wikimedia.org/wiki/File:M_Zauneidechse1_Edit1.jpg, CC BY-SA 3.0, accessed: 2022-04-11. Photo of adult *Lacerta viridis*: Uoaei1 (2014-04-12), via https://commons.wikimedia.org/w/index.php?curid=39840199, CC BY-SA 4.0, accessed: 2022-04-11

In this study, the following hypotheses will be investigated: Since no feeding or hunting specializations were mentioned in the literature for the three species, it was assumed that no heterochrony in embryonic jaw development would be identified. In contrast, because vision is a very important sense for lacertids, not only for foraging or avoiding predators, but also for intraspecific communication, Martin et al. (2014) have suggested "that the visual system and visual signals might co-evolve." Thus, variations in eye genesis between species with different lifestyles were expected. Similarly, pronounced interspecific embryonic differences in limb development were expected among non-climbing or only occasionally climbing species. Some heterochrony in scale development, possibly related to microornamentation based on habitat preference was also anticipated, as suggested by Arnold (2002).

2 | MATERIAL AND METHODS

2.1 | Species

2.1.1 | The European green lizard *Lacerta viridis*

Numerous populations of the European green lizard *Lacerta viridis* are distributed throughout Europe, up to elevations of 2000 m above sea level. These lizards characteristically inhabit a shrubby habitat, such as that found on roadsides, forest edges, or clearings (Engelmann et al., 1986). Shrubs are of great importance to the species and are used both for sunbathing and protection from predators (Böhme, 1984). Although it is an occasional climber, *L. viridis* disappears when the habitat becomes overgrown, and the potential for thermoregulation in sun-exposed areas is lost (Kirmse, 1990). *L. viridis* does not occur in steppes or coniferous forests, and feeds on all types of insects, especially beetles, but also eats eggs, juvenile mammals, and small reptiles (Böhme, 1984).

With a snout-vent length of up to 13 cm and a very long tail that extends up to 40 cm, *L. viridis* is one of the largest lizards among European species (Figure 1, Engelmann et al., 1986). Adults of both sexes are colored shades of green, ranging from yellowish to blue, and sometimes have a dark pattern; males often have blue throats, particularly during the breeding season (Engelmann et al., 1986). Juveniles are brown, usually without a pattern, and blend in with their environment (Böhme, 1984). Böhme (1984) attributes the extremely variable incubation time for *L. viridis* (other authors mention a period between 50 and 100 days) to their large distribution area and the consequent variation in incubation parameters (Engelmann et al., 1986; Hill & Klepsch, 2008).

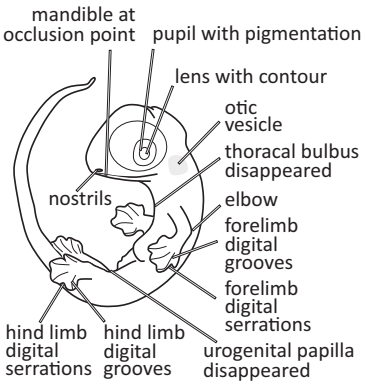

FIGURE 2 Selected standard event system (SES) characters coded in this study illustrated for a mid-term embryo (image modified from Yaryhin & Werneburg, 2017: fig. 1a). For more details on SES-characters see: https://en.wikipedia.org/wiki/Standard_Event_System [accessed: 2022-04-11]

2.1.2 | The sand lizard *Lacerta agilis*

Distributed and common in almost all European countries, the sand lizard *Lacerta agilis* is one of the few reptiles that are described as synanthropic, meaning that it thrives in anthropogenic landscapes with structures, such as road and railway embankments, parks, cemeteries, and gardens (Böhme, 1984).

Many subspecies exhibit a wide variety of colors in all shades of green and brown and patterns from nearly solid to dots and stripes, with strong sexual dimorphism (Böhme 1984; Engelmann et al., 1986). *L. agilis* is a medium-sized lizard (Figure 1), reaching a snout-vent length of approximately 11 cm with a total length of up to 27.5 centimeters (Böhme, 1984; Engelmann et al., 1986).

The sand lizard feeds on arthropods and lizard eggs and occasionally exhibits cannibalistic behavior (Böhme, 1984). Similar to *L. viridis*, the incubation time of *L. agilis* is variable; known values range from approximately 32–36 days at very high temperatures (28°C) to over 60–75 days (Peter, 1904) or even 70–90 days (Märtens, 1999) at lower temperatures.

2.1.3 | The Caucasian rock lizard *Darevskia armeniaca*

The Caucasian rock lizard, *Darevskia armeniaca*, has been described and taxonomically reclassified several times. Consequently, there is some ambiguity in the nomenclature and common descriptions. Girnyk et al. (2018) state that the Caucasian rock lizard "originated through interspecific hybridization between the closely related sexual *Darevskia mixta* and *Darevskia valentini*," which, according to Darevsky (1966), "apparently took place in forest refuges during the Quaternary glaciation of the Caucasus." Today, the distribution of *D. armeniaca* extends from northwestern Turkey through South Georgia and northern Armenia to northwestern Azerbaijan (Bischoff, 2003). It was intentionally introduced into Ukraine in 1963 with the aim to "study the process of acclimatization and hybrid complexes of lizards" (Nekrasova & Kostiushyn, 2016).

Bischoff (2003) has described its occurrence as linked to rocky habitats, such as rivers or roadbanks, at elevations from above 1350 m to above 2200 m. In contrast to other lacertids, purely female populations appear extraordinarily nonviolent towards each other (Karmyshev & Yaryhin, 2013). Adults are green or olive in color with a black pattern and a white or yellow belly (Figure 1), and hatchlings are

coppery with a green tail (Bischoff, 2003). Karmyshev and Yaryhin (2013) have reported an incubation period of 66 days.

2.1.4 | Outgroup comparison

For the outgroup comparison in the phylogenetic analysis, the black and white tegu *Salvator merianae* (Teidae) was chosen because it is phylogenetically close to Lacertidae (Streicher & Wiens, 2017), and it has a more or less generalized lizard anatomy without limb reduction (e.g., snakes, amphisbaenians, and skinks) or large eyes (e.g., geckos), and very detailed embryonic data are available for this species (Iungman et al., 2008).

2.2 | Embryonic sampling

To obtain embryonic material of the lacertid species, gravid females of all species were caught in their natural habitats in Ukraine from 2007 to 2011 (Figure 1). The capture of animals is allowed if they are not listed in the Red Data Book of Ukraine (Akimov, 2009). *Lacerta viridis* was added to the list in 2009, but was captured before that, in 2007. The female lizards were kept in terraria where they successfully laid their eggs. Animal husbandry was approved by the Ethics Committee of the Schmalhausen Institute of Zoology NAS of Ukraine. The eggs were incubated on moistened vermiculite at temperatures ranging from 21 to 23°C (Karmyshev & Yaryhin, 2013; Yaryhin & Werneburg, 2018). The maximum incubation times were 85 days, 65 days, and 66 days for *L. viridis*, *L. agilis*, and *Darevskia armeniaca*, respectively. For the latter, the authors mention "a rather large number of embryonic malformations (up to 7%), and twins were also found twice in the eggs", which they account to their parthenogenic mode of reproduction (Karmyshev & Yaryhin, 2013). Because almost no genetic mixing by mating occurs in parthenogenetic species (Darevsky et al., 1978), acquired mutations accumulate in the lineage, causing an unusually high rate of malformed embryos. No malformed embryos of any species were analyzed in the present study, but data from embryos with delayed development were used if no other embryos were available. As gravid females were collected from the field, whether males were involved in reproduction cannot be stated with certainty. Nevertheless, it is important to note that neither more nor less intraspecific variation was detected in *D. armeniaca* when compared to both *Lacerta* species.

The embryos obtained were then fixed in formalin and stored in 4% buffered formalin, 100% methanol, or 70% ethanol. Some embryos were stained with phosphotungstic acid (PTA) to prepare them for another study using μCT scans.

2.3 | Data sampling

2.3.1 | Photography

The specimens were photographed using a Leica Z16 Apo trinocular microscope (Leica Biosystems Technology, Stuttgart, Germany) equipped with a camera and refined using Image-Pro Plus software (Media Cybernetics, Rockville, USA). If possible, dorsal, ventral, and lateral views were obtained, as proposed by Werneburg (2009) (some specimens were broken, twisted, or too small). An example is shown in Figure 1.

2.3.2 | Discrete character coding

To enable quantitative and qualitative comparison of inter- and intraspecific variation in embryogenesis, Werneburg (2009) has developed the "Standard System to Study Vertebrate Embryos" (SES). The system provides a comprehensive catalogue of more than 100 homologous external developmental characters in various complexes, such as the eye, pharyngeal arch, and limb morphology. By carefully examining every specimen and assigning observable characters, one receives a discrete, comparable description of an embryonic series, which may easily be supplemented by new characters or specimens, as shown in Figure 2. The SES has been expanded throughout the last few years by Werneburg et al. (2016) and the updated database can be accessed herein: https://en.wikipedia.org/wiki/Standard_Event_System (access: 2022-04-11). As initial development of embryos takes place in the oviduct, because of the sampling technique described above, there was only access to embryos of advanced development, so not all SES characters could be observed. Some characters described in the SES did not apply to reptiles or lacertids. Therefore, the following SES-characters were not documented: complexes A, B, D, U, V, W, X, Y, Z, G4, H6, I1, L23, L24, L29, L30, M11, N1-N4, S1-2, and T3 (Werneburg, 2009; Werneburg et al., 2016).

In the present study, 15 *Lacerta viridis* embryos, 33 *L. agilis* embryos, 36 *Darevskia armeniaca* embryos, and 28 *Salvator merianae* embryos taken from the literature (Iungman et al., 2008) were examined. For complete information and SES data of the specimens, see Tables S1–S3.

2.3.3 | Data comparison among species and phylogenetic analysis

Despite the different incubation lengths given in the literature, the age of each specimen has been scaled by the maximum incubation time given by Karmyshev and Yaryhin (2013), which were obtained through controlled and constant conditions, to make comparisons of the timing of developmental characters possible. Werneburg et al. (2016) have discussed whether the birth and hatching of different animals may be homologous, which would be crucial for SES coding, and answered positively, as the breach of the amnion is a homologous event for all amniotes. In that case, it was decided against using birth as the maximal value, as mammals are very differently developed at birth; that is, on a spectrum of precocial to altricial. As lizards are precocial animals and basically 'miniature adults' apart from coloring, it was used here because the four species are similarly sized at hatching. This way, all events were scaled resulting in values between '0' (i.e., egg lay) and '1' (i.e., hatch) for every

developmental character in every species. Using conception as a starting point for comparison would have been a better proxy. However, all three compared species were taken from the field and stable life conditions of the females there could not be guaranteed. With fluctuating temperatures, development may last longer or be shorter (diapauses). As such, for the most reliable comparison in lizards, it was decided to consider egg laying as a starting point of compared development because the incubation conditions were controlled and stable.

To examine intraspecific variation, the earliest and latest values and the arithmetic mean for the timing of each character were compared. For the comparison of interspecific variation, the earliest value was used instead of the arithmetic mean because many characters persist for a long period of time after their first appearance, which affects the mean calculation. This procedure also circumvented the problem arising from the variable time the egg remained in the uterus until it was laid. Since each specimen only shows one continuous trait at a time within a complex, and trends within a complex were compared instead of individual traits, a robust developmental trend for each species was obtained. Individual specimens that were developmentally delayed owing to malformations were immediately conspicuous by external features and compared to conspecifics. Hence, for a proper interspecific comparison, only the earliest appearance of a character was chosen (see Werneburg et al., 2016).

With these values, a phylogenetic analysis using Mesquite version 3.61 (Maddison & Maddison, 2018), applying the continuous character and square change parsimony approach (Felsenstein, 1985) was performed (as in Germain and Laurin, 2009). This resulted in ancestral state reconstructions: the values for the ancestral timing of the characters for the 'genus' *Lacerta* and for the ancestor of all 'Lacertidae' (Table S4, Figures 3–6).

The time of evolutionary divergence of the four species was calculated using timetree.org (last access: 2021-10-01) from Kumar et al. (2017), which uses the best estimates from a variety of molecular studies. The calculation resulted in the following divergence times: *Lacerta agilis*/*L. viridis* = 21.7 million years, *Darevskia armeniaca*/*Lacerta* = 44.8 million years, *Salvator merianae*/Lacertidae = 168 million years.

For comparison, the ancestral sequences of Lacertidae and the individual sequences of the three lacertid species were plotted in four diagrams (Figures 3–6). The sequence data were sorted by the timing of character appearance in the lacertid ancestor.

3 | RESULTS

3.1 | Intraspecific variation in developmental sequence

Each of the species studied here exhibited some degree of intraspecific variation; that is, the same embryonic characters were observed to appear and/or disappear at different times during ontogeny. Statistical tests on this variation were not performed because there were too few data points for a sufficient analysis. Therefore, this study represents an exploratory, rather than a quantitative assessment (as in [Parsi-Pour & Werneburg, 2019]), often the only approach to deal with rare embryological data. To estimate intraspecific variation, the earliest and latest occurrence and arithmetic mean of the timing of SES traits were presented for the three lacertids (Figures 3–5, Table S4). Developmental sequences were sorted according to the reconstructed ancestral states of all three species observed in this study.

The Armenian rock lizard *Darevskia armeniaca* (Figure 3, Table S1) was highly variable in the temporal sequence of the visual and auditory organ systems, particularly in the extremities. As discussed in more detail in the Methods section, many specimens of *D. armeniaca* had malformations or were generally delayed in their development; for example, they seemed 'normally developed', but were older than expected. One noteworthy example is DA80, the only specimen in which digital grooves were observed in the forelimbs ('L15') and hind limbs ('L16'). Therefore, the values for these characters were higher than those for 'L19. Finger' or 'L20. Toe' and were treated as outliers in intra- and inter-specific comparisons. When compared to the development of the reconstructed ancestral state, *D. armeniaca* often seemed delayed at the beginning of development, but completed its growth as the earliest of the species.

A few specimens were available for the green lizard *Lacerta viridis* (Figure 4, Table S2). In several cases, SES characters could only be observed in one embryo, and many were absent altogether, making the dataset for this species the sparest. This also affected observable intraspecific variation. Nevertheless, the development of sensory organs exhibited a great deal of temporal variation, similar to limb growth. The oldest specimen (LV8) had no scales, but this was probably because of its poor preservation. With a few exceptions, the development of *L. viridis* was delayed compared to that of the ancestral state reconstruction.

In contrast, the sand lizard *L. agilis* (Figure 5, Table S3) began embryonic development earlier than the reconstructed ancestral state, but growth appeared to slow as it progressed, and organogenesis was completed later. For *L. agilis*, many specimens were well distributed throughout embryogenesis, so there were few problematic characters. 'P4, the mandibular arch bud midline eye' appeared to be delayed, but as only one specimen displayed this character it was treated as an outlier. The development of the hind extremities occurred later than that of the fore extremities.

3.2 | Interspecific variation and evolutionary change

The earliest values for all three species, as well as ancestral state reconstruction, are shown in Figure 6, illustrating the heterochronic embryonic development.

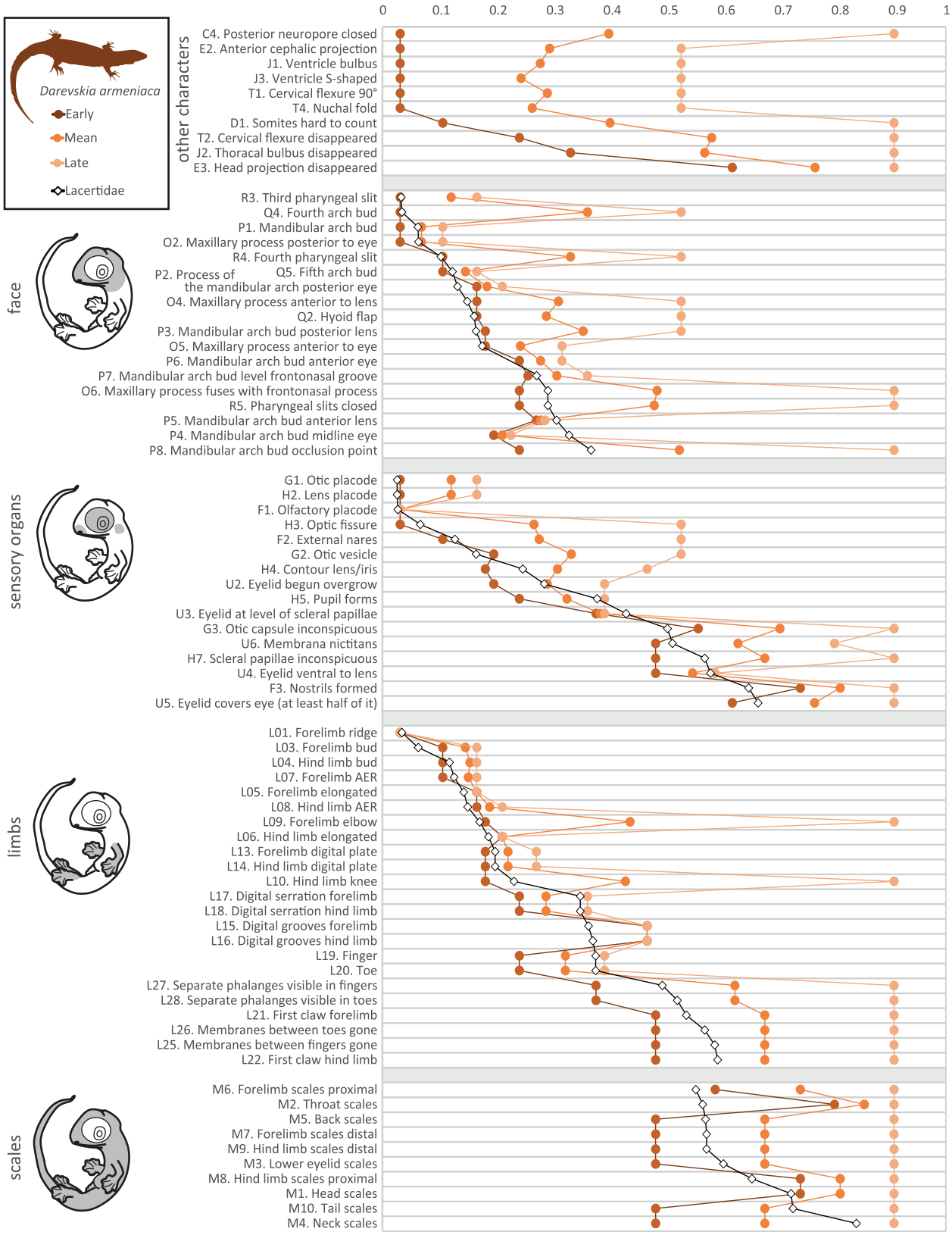

FIGURE 3 Intraspecific variation in the timing of embryological development of the Armenian rock lizard *Darevskia armeniaca*, scaled by hatch = 1, and the reconstructed ancestral lacertid condition (Lacertidae). In addition to the four illustrated body region categories (face, sensory organs, limbs, and scales), also early ontogenetic characters are listed for which no ancestral lacertid states could be calculated because the outgroup is missing this information. Abbreviations of characters such as "P1. Mandibular arch bud" or "L04. Hind limb bud" refer to the official SES numeration and SES character abbreviation system, as introduced by Werneburg (2009) and Werneburg et al. (2016) and as summarized at: https://en.wikipedia.org/wiki/Standard_Event_System [accessed: 2022-04-11]

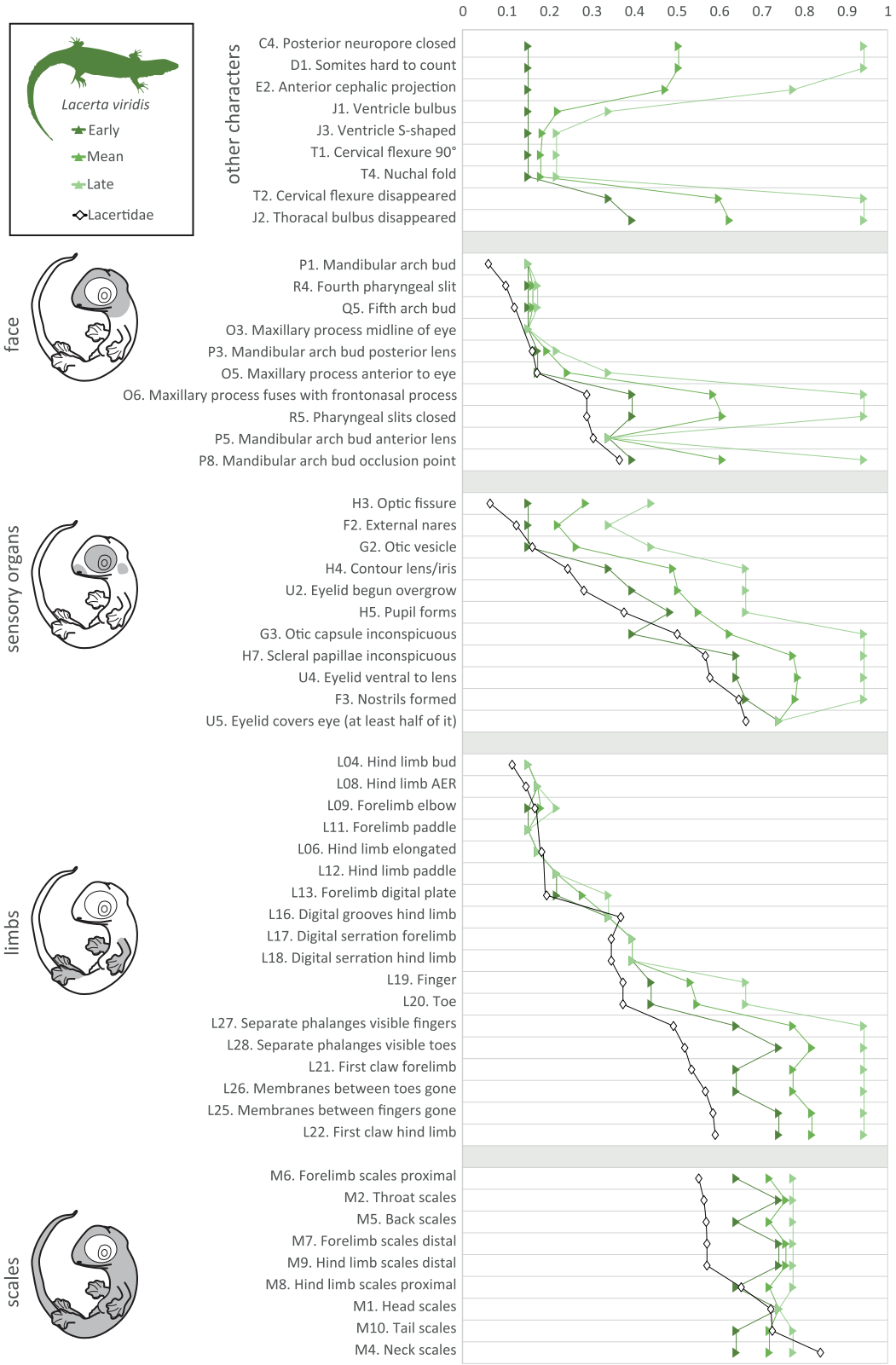

FIGURE 4 Intraspecific variation in the timing of embryological development of the green lizard *Lacerta viridis*, scaled by hatch = 1, and the reconstructed ancestral lacertid condition (Lacertidae). For abbreviations, see the legend of Figure 3

The ontogeny of the face, that is, the snout and pharyngeal region, is dominated by the growth of the jaw, which originates from the first pharyngeal (mandibular) arch that forms "a dorsal maxillary and a ventral mandibular process' (Werneburg, 2009). These processes move from the posterior to the anterior of the eye, where the former fuses with the nasal region and both extend anteriorly until

FIGURE 5 Intraspecific variation in the timing of embryological development of the sand lizard *Lacerta agilis*, scaled by hatch = 1, and the reconstructed ancestral lacertid condition (Lacertidae). For abbreviations, see the legend of FIGURE 3

the occlusion point of the maxilla and mandible is reached (Werneburg 2009). Initially, a similar pattern was recognizable among the studied species; at the time of oviposition, some pharyngeal slits and arches were developed and rapidly closed and dislimned as the maxilla and mandible moved anteriorly. Contrary to our first hypothesis of simultaneous 'jaw development' in all three lacertid species,

closure of pharyngeal slits, fusion of the maxillary process with the nasal region, and finally jaw closure was first achieved by *Darevskia armeniaca*, in the first third of embryogenesis. In contrast, both *Lacerta* species completed jaw formation at approximately the same time in the second third of the incubation period, with *L. viridis* occurring a little earlier.

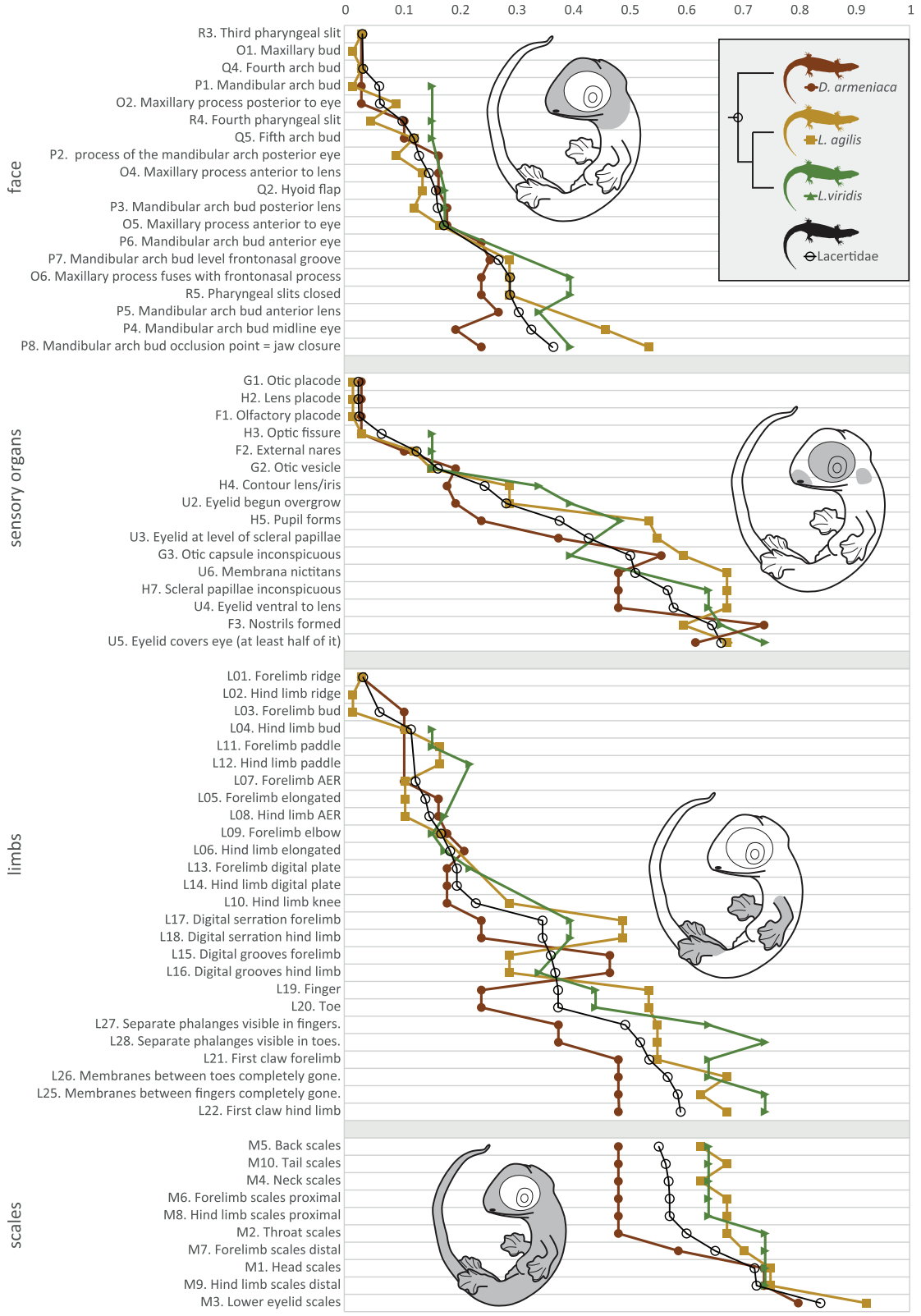

FIGURE 6 Interspecific variation in the earliest appearance of embryological characters (face, sensory organs, limbs, and scales) in the three species, *Darevskia armeniaca*, *Lacerta viridis*, and *L. agilis*, scaled by hatch = 1, and the reconstructed ancestral lacertid condition (Lacertidae). For abbreviations, see the legend of FIGURE 3

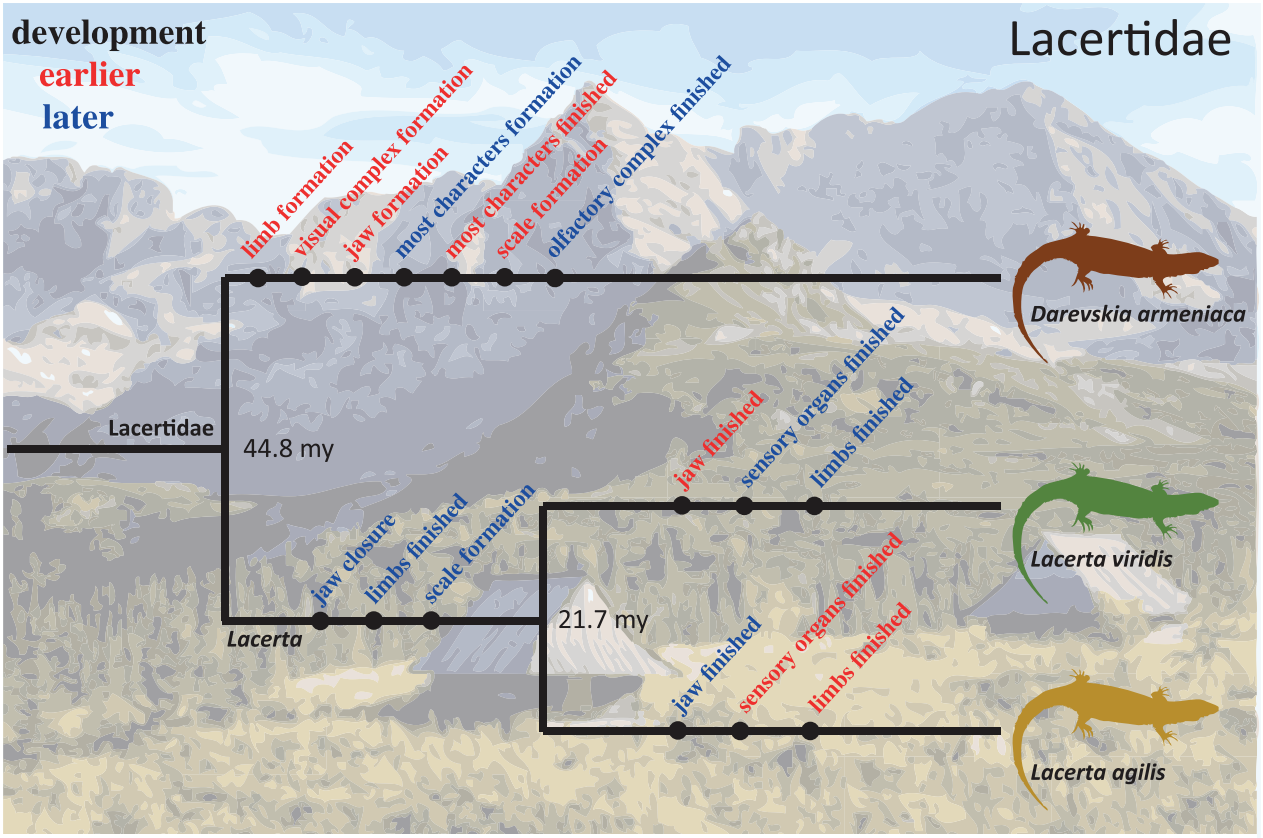

FIGURE 7 Habitat range and phylogenetic relationship, including the time of evolutionary divergence for the species *Darevskia armeniaca*, *Lacerta viridis*, and *L. agilis*. Time in million years. Derived characters on the tree represent a summary of the findings of this study. Red writing indicates earlier, blue writing indicates later character appearance in ontogeny. Characters on the tree present summaries of one or more standard event system (SES)-character development(s) that are illustrated in Figures 3 and 4. Landscape illustration in the background is a personal adobe illustrator artwork based on a photo indicating the habitat for the respective species with *Darevskia armeniaca* living in mountainous environments. *Lacerta viridis* inhabits a characteristically shrubby habitat, such as roadsides, forest edges, or clearings. *L. agilis* thrives in anthropogenic landscapes with structures, such as road and railway embankments, parks, cemeteries, and gardens

Regarding the development of facial senses, interspecific differences were expected in the visual and nasal complex. Accordingly, the auditory complex developed quite similarly in all three species. In contrast, but consistent with our second hypothesis, the visual system exhibited interspecific differences in its development, with *D. armeniaca* displaying both the direct visually related characters and those of the later-emerging eyelid complex much earlier in development. *D. armeniaca* was the last and *L. agilis* was the first species to have fully formed nostrils.

In accordance with the expected interspecific variation in limb development, the most striking heterochrony was observed in the character complexes associated with locomotion. Limb development began immediately after oviposition in all species and continued into the second third of embryogenesis. While *D. armeniaca* completed the development halfway through the incubation period, *L. agilis* took just until the last third and *L. viridis* unexpectedly took the longest.

When examining scale development, the observed interspecific differences were consistent with our fourth hypothesis, as it was expected to find heterochrony in this character complex. Scale onset seemed to be connected to the completion of limb development, and consequently, *D. armeniaca* started and finished scale growth first. This followed the general pattern of all three species, according to which scales grew only after the body had formed and grown. Scales first appeared on the back and neck, whereas the scales on the lower eyelid grew last.

4 | DISCUSSION

Intraspecific variation among lacertid species was observed, particularly in limb, facial, and scale development. These variations were mirrored in interspecific differences, as they were most likely related to postnatal adaptations, implying developmental penetrance.

It should be noted that the 'early equals importance' rule (Huxley, 1932; Mehnert, 1897; Mehnert, 1898) does not necessarily mean that the early appearance of a character correlates with the size of a fully developed anatomical feature. It may also be related to structural differentiation; for example, increased complexity of internal anatomy, such as diversification of muscles or ossification (Werneburg & Sánchez-Villagra, 2009). As discussed by Werneburg et al. (2015), this also allows for the execution of ontogenetic

functions that occur only for a limited period of time (see also Werneburg et al., 2013).

Cordero et al. (2021) have concluded that Lacertini differs in limb development only after hatching by comparing the quantitative and metrical data of very similarly sized animals. In the present study, discrete and qualitative data of morphology were compared. Therefore, the results of the two studies do not necessarily contradict each other, but are also not strictly comparable. Furthermore, not only late limb development, where whole limb length is measured (Cordero et al., 2021), but also the earliest states of limb differentiation have been examined, including limb ridge, limb bud, and digital serration, as well as specific differentiations, such as finger formation.

4.1 | Facial development

4.1.1 | Formation of the jaw

All three lacertid species studied herein feed on a similar, mainly insectivorous diet, and no specialization has been mentioned in the literature for any of the species (Böhme, 1984, 1984). Therefore, no embryological differentiation of jaw formation was expected. Surprisingly, the data showed that *Darevskia armeniaca* completed closure of the maxillary and mandibular processes, as well as pharyngeal slits, considerably earlier than the other species studied during the first third of embryogenesis (Figure 7). Further research on adult and hatchling dietary specifications might reveal a link to the observed interspecific differences. However, since the formation of facial features is one of the processes that begin earliest in organogenesis (Werneburg 2009), and most specimens in this study were further developed, these results must be verified by comparing younger specimens.

4.1.2 | Development of facial sensory organs

Regarding the development of the external sensory organs of the head, noticeable intra- and interspecific variation was observed in eye formation (Figure 7). Research on visual sense in lacertids has only just begun, but as Martin et al. (2014) have suggested, it may be of much greater importance than previously thought, including for intraspecific communication. For example, some species display visual signals in the ultraviolet or infrared range, which requires retinal specialization (Martin et al., 2014). In this study, *D. armeniaca* achieved eye development earlier than both *Lacerta* species, strongly suggesting developmental penetrance of a specialized visual system.

Interestingly, *D. armeniaca* was the last, and *L. agilis* was the first species to exhibit fully formed nostrils. As suggested by Baeckens et al. (2015), chemical signaling in lizards may be subject to strong sexual selection and may be particularly important to males. Considering that the Armenian rock lizard is a parthenogenic species, the delayed formation of the nostril suggests that olfaction might play a minor role in this species.

4.2 | Locomotion

The most striking difference among the three lacertid species is the way they move in their different habitats (Figure 7). Therefore, limb development was expected to vary embryonically, and, indeed, both intraspecific and interspecific variation was observed. *Darevskia armeniaca*, as a mountain dweller and consequently an actively climbing species, completed limb development earlier than *Lacerta viridis*, *L. agilis*, and also earlier than the reconstructed ancestral sequence of lacertid development. Notably, *L. viridis*, as an occasional climber in the lower shrub layer, completed limb development later than *L. agilis*, which remains on the ground in the herbaceous layer and does not climb (Böhme, 1984). Apart from length (Cordero et al., 2021), there are no obvious external anatomical differences in the limbs of adults between all lizard species. However, based on its climbing behavior, it is very likely that *D. armeniaca* has different and longer internal anatomical specializations in the limbs, including myology and degree and mode of ossification (Bischoff, 2003).

4.3 | Scales

To protect the animal's body, scales must be fully developed before hatching. However, because scales do not grow or multiply, shedding is required to make room for the growing body (Spearman, 1973). Because the embryo cannot shed its skin (Spearman, 1973), it is crucial for it to complete growth processes earlier than scale formation. Interestingly, the onset of scale growth was observed in areas that do not experience changes later in embryogenesis, such as the back and neck. These conditions limit the applicability of the 'early equals importance rule'.

In the present study, scale formation started at the same time as the completion of limb development in all species. However, while *Lacerta agilis* and *L. viridis* appeared to develop scales similarly in the last third of embryogenesis, *Darevskia armeniaca* finished scale formation earlier (Figure 7).

According to Arnold (2002), scale microornamentation in lacertids is linked to the habitat and behavior of the species and exhibits two opposite characteristics. The more ancestral mode would enhance smoothness to avoid soiling and facilitate movement in narrow crevices, which also increases light reflection (Arnold, 2002). A more derived scale surface would reduce smoothness to avoid attracting predators and does appear dorsally in *L. viridis* and *L. agilis* (Arnold, 2002). Reduced smoothness is associated with "dry habitats or when they live away from the ground, both situations where soiling is unlikely to be a great problem" (Arnold, 2002). It is not known which sort of microornamentation appears in *D. armeniaca*, but given their close association with rocks and their montane habitat at high elevations, both the ancestral smooth and the derived reflection-reducing pattern seem likely. Comparing the embryological data, it seemed likely that as both *Lacerta* species completed scale growth later and have more derived scale microornamentation, *D. armeniaca*

probably has a more ancestral one. This would also fit their lifestyle, hiding in rock crevices.

4.4 | Developmental penetrance

We hypothesized there would be intra- and interspecific differences in embryonic development, the latter representing an embryonic pre-adaptation to the later lifestyle and anatomical adaptation of adult lizards of *Darevskia armeniaca*, *Lacerta agilis*, and *L. viridis*. Using the SES approach developed by Werneburg (2009) to make continuous embryonic differentiation comparable, interspecific variation was identified, particularly in limb development, but also in scale, sensory, and facial development. Therefore, it seems that, although separated for only 44 million years, changes in adult anatomy have clearly penetrated into embryogenesis.

The main results concern the differences in limb development. In this regard, *D. armeniaca* developed limbs considerably earlier, suggesting a specialized adaptation to its rocky habitat and climbing lifestyle. Since no external anatomical differences of the limbs were evident in adults, this should be investigated further by studying their extremities, especially internal morphological differentiation.

In all species, the development of scales occurred within a very short interval from their first appearance and their completion just before hatching, although they are very important to both the hatchlings and adults (Spearman, 1973). This is due to the fact that the whole body must be developed before scales appear, as after scales cover the animal, growth is only possible by shedding, which is a well-developed feature in squamates (Spearman, 1973). Nevertheless, there were differences among the species, with *D. armeniaca* developing scales first, which was most likely related to adaptations, such as scale microornamentation.

Surprisingly, a large difference was found in the timing of facial development, namely, in the growth of the jaw and in the genesis of the eye and its eyelids. In both cases, *D. armeniaca* exhibited the most rapid development, suggesting a developmental penetrance of specific adaptations that have yet to be discovered. It is very likely that there is some sort of specification in *D. armeniaca* for both the diet and visual system, perhaps related to its relatively small distribution range and rocky habitat.

The early development of *D. armeniaca* indicated mature hatchlings compared to that of other lacertid lizards. This may be particularly advantageous in extreme conditions given their montane habitat, where only a short period between long winters is suitable for lizard activity, but young hatch only in autumn (Nekrasova & Kostiushyn, 2016).

4.5 | Conclusions

Reptiles are a useful model to address fundamental questions regarding evolutionary mechanisms because most lay eggs, which allows for good access to numerous embryos at different developmental stages for research. In addition, some of their clades are extremely diverse and radiate into "empty niches" within a few decades (Stuart et al., 2014). One example is Lacertidae, in which rapid diversification supported by developmental penetrance has manifested itself in as little as 44 million years (Kumar et al., 2017).

Intraspecific variation was observed in the timing of ontogeny prior to hatching during the development of the face, sensory organs, locomotor system, and scales. This suggested sufficient variation to cause natural selection at the earliest stages of ontogeny, thereby enabling speciation by following the 'early equals importance' rule.

The observation of concordant interspecific variation further supports our hypotheses (Figure 7). In *D. armeniaca*, an earlier jaw development, an earlier formation of the visual complex, a later completion of the olfactory complex, a very early limb, and scale development was observed when compared to those of the ancestral lacertid condition. In general, most characters showed a late onset of formation, but an early completion. Compared to that of the ancestral Lacertidae condition, *Lacerta* was characterized by later jaw closure, formation of sensory organs, and limb and scale development. Compared to that of the ancestral *Lacerta* condition, *L. viridis* showed later formation and earlier completion of jaw and limb development. Its sensory organ and scale development were delayed compared to those of *Lacerta*. Compared to that of the ancestral *Lacerta* condition, *L. agilis* showed earlier formation and later completion of jaw development, while sensory organ development took place earlier. In contrast, scale development was delayed and the limbs developed similar to the ancestral *Lacerta* condition (Figure 7).

These results are inconsistent with previous studies on lacertid limb development, in other words, they were elusive in previous comparative studies based on purely metric data (Cordero et al., 2021). This highlights the importance of multiple data sources to draw robust conclusions about evolutionary change. Therefore, the stable observation of intra- and interspecific patterns of variation across whole-body development was interpreted as an indication of the importance of using discrete data sources and a more qualitative approach to draw conclusions about evolutionary change. Especially since development is a continuous process that cannot be measured using quantitative measurements alone. This conclusion was based on these observations that although no dietary or hunting specialization has been mentioned in the literature, heterochrony was identified in the embryonic jaw development of the three species. In addition, the differences in the development of the facial sensory system, as well as the limbs and scales, suggested deep developmental penetrance of adaptations to slightly different lifestyles and habitats, which might account for the success of the diverse lacertids.

ACKNOWLEDGMENTS

We wish to thank Gerardo Antonio Cordero (Lisbon) for discussions. Two anonymous reviewers are thanked for their suggestions to improve the manuscript. This study was supported by DFG-funds WE 5440/5-1 and WE 5440/6-1 to I.W.

Open Access funding enabled and organized by Projekt DEAL.

CONFLICT OF INTEREST

None.

AUTHOR CONTRIBUTIONS

Conceptualization: IW, OY, XS.

Collected specimens: OY.

Analyses: XS, OY.

Wrote paper: XS, IW.

ORCID

Xenia Schlindwein https://orcid.org/0000-0002-4224-6506

Oleksandr Yaryhin https://orcid.org/0000-0003-0363-2057

Ingmar Werneburg https://orcid.org/0000-0003-1359-2036

REFERENCES

Akimov, I. A. 2009 (ed.). Red book of Ukraine. Animals. Kyiv: Globalconsulting. [Original title: Акімов, І. А. (за ред.). 2009. Червона книга України. Тваринний світ. Київ:, 2009].

Arnold, E. (2002). History and function of scale microornamentation in lacertid lizards. *Journal of Morphology*, *252*, 145–169.

Baeckens, S., Edwards, S., Huyghe, K., & Van Damme, R. (2015). Chemical signalling in lizards: An interspecific comparison of femoral pore numbers in Lacertidae. *Biological Journal of the Linnean Society*, *114*, 44–57.

Bickelmann, C., Mitgutsch, C., Richardson, M. K., Jiménez, R., De Bakker, M. A. G., & Sánchez-Villagra, M. R. (2012). Transcriptional heterochrony in talpid mole autopods. *EvoDevo*, *3*, 16.

Bischoff, W. (2003). Die Eidechsenfauna Georgiens. Teil II: Die Gattung *Darevskia*. *Die Eidechse*, *14*, 65–93.

Böhme, W. (1984). Lacerta agilis - *Zauneidechse In Handbuch der Reptilien und Amphibien Europas*, *Band 2/1*, *Echsen II* (Lacerta) (p. 156). AULA-Verlag.

Cordero, G. A., Maliuk, A., Schlindwein, X., Werneburg, I., & Yaryhin, O. (2021). Phylogenetic patterns and ontogenetic origins of limb length variation in ecologically diverse lacertine lizards. *Biological Journal of the Linnean Society*, *132*, 283–296.

Darevsky, I. S. (1966). Natural parthenogenesis in a polymorphic group of Caucasian rock lizards related to *Lacerta saxicola* Eversmann. *Journal of the Ohio Herpetological Society*, *5*, 115–152.

Darevsky, I. S., Kupriyanova, L. A., & Bakradze, M. A. (1978). Occasional males and intersexes in parthenogenetic species of Caucasian rock lizards (genus *Lacerta*). *Copeia*, *1978*, 201–207.

Engelmann, D. W.-E., Fritzsche, J., Günther, D. S. R., & Obst, D.-B. F. J. (1986). *Lurche und Kriechtiere Europas*. Ferdinand Enke Verlag.

Felsenstein, J. (1985). Confidence limits on phylogenies: An approach using the bootstrap. *Evolution*, *39*, 783–791.

Germain, D., & Laurin, M. (2009). Evolution of ossification sequences in salamanders and urodele origins assessed through event-pairing and new methods. *Evolution & Development*, *11*, 170–190.

Girnyk, A. E., Vergun, A. A., Semyenova, S. K., Guliaev, A. S., Arakelyan, M. S., Danielyan, F. D., Martirosyan, I. M., Murphy, R. W., & Ryskov, A. P. (2018). Multiple interspecific hybridization and microsatellite mutations provide clonal diversity in the parthenogenetic rock lizard *Darevskia armeniaca*. *BMC Genomics*, *19*, 979.

Hamrick, M. W. (2001). Primate origins: Evolutionary change in digital ray patterning and segmentation. *Journal of Human Evolution*, *40*, 339–351.

Hill, J., & Klepsch, R. (2008). *Kartierung der Reptilienfauna des Nationalparks Thayatal (Niederösterreich) an ausgewählten Standorten unter besonderer Berücksichtigung der Würfelnatter (Natrix tessellata) und der Smaragdeidechse* (Lacerta viridis). Nationalpark Thayatal GmbH.

Huxley, J. (1932). *Problems of relative growth*. Methuen & Co.

Iungman, J., Piña, C. I., & Siroski, P. (2008). Embryological development of *Caiman latirostris* (Crocodylia: Alligatoridae). *Genesis*, *46*, 401–417.

Karmyshev, Y. V., & Yaryhin, D. O. (2013). Reproductive features of several Ukrainian true lizards (Lacertidae) [Original title: Репродуктивные особенности некоторых настоящих ящериц (Lacertidae) Украины]. *Ukrainian Journal of Ecology*, *1*, 59–64.

Kirmse, W. (1990). Die Smaragdeidechse (*Lacerta viridis*) in Brandenburg: Bestand und Schutzmaßnahmen. *Die Eidechse*, *1*, 10–12.

Kumar, S., Stecher, G., Suleski, M., & Hedges, S. B. (2017). TimeTree: A resource for timelines, timetrees, and divergence times. *Molecular Biology and Evolution*, *34*, 1812–1819.

Maddison, W. P. & Maddison, D. R. https://www.mesquiteproject.org/

Maier, W. (1999). On the evolutionary biology of early mammals - with methodological remarks on the interaction between ontogenetic adaptation and phylogenetic transformation. *Zoologischer Anzeiger. Festschrift D. Starck*, *238*, 55–74.

Märtens, B. 1999. Demographisch ökologische Untersuchung zu Habitatqualität, Isolation und Flächenanspruch der Zauneidechse (*Lacerta agilis*, Linneaus, 1758) in der Porphyrkuppenlandschaft bei Halle (Saale).

Martin, M., Le Galliard, J.-F., Meylan, S., & Loew, E. (2014). The importance of ultraviolet and near-infrared sensitivity for visual discrimination in two species of lacertid lizards. *The Journal of Experimental Biology*, *218*, 458–465.

Mehnert, E. (1897). *Kainogenesis als Ausdruck differenter phylogenetischer Energien*. G. Fischer.

Mehnert, E. (1898). *Biomechanik erschlossen aus dem Principe der Organogenese*. G. Fischer.

Nekrasova, O., & Kostiushyn, V. (2016). Current distribution of the introduced rock lizards of the *Darevskia* (Saxicola) complex (Sauria, Lacertidae, Darevskia) in Zhytomyr region (Ukraine). *Vestnik Zoologii*, *50*, 225–230.

Parsi-Pour, P., & Werneburg, I. (2019). Developmental differences between two marine turtle species and potential consequences for their survival at hatching. *Zoology (Jena, Germany)*, *136*, 125708.

Peter, K. (1904). Normentafel zur Entwicklungsgeschichte der Zauneidechse (*Lacerta agilis*). In F. Keibel (Ed.), *Normentafeln zur Entwicklungsgeschichte der Wirbeltiere* (Vol. Heft 4). Gustav Fischer.

Raff, R. (1996). *The shape of life*. University Press.

Richardson, M. K. (1999). Vertebrate evolution: The developmental origins of adult variation. *BioEssays*, *21*, 604–613.

Richardson, M. K. (2022). Theories, laws, and models in evo-devo. *Journal of Experimental Zoology B*, *338*, 36–61.

Spearman, R. I. (1973). *The integument: A textbook of skin biology*. Cambridge University Press.

Streicher, J. W., & Wiens, J. J. (2017). Phylogenomic analyses of more than 4000 nuclear loci resolve the origin of snakes among lizard families. *Biology Letters*, *13*, 1–4.

Stuart, Y. E., Campbell, T. S., Hohenlohe, P. A., Reynolds, R. G., Revell, L. J., & Losos, J. B. (2014). Rapid evolution of a native species following invasion by a congener. *Science*, *346*, 463–466.

Werneburg, I. (2009). A standard system to study vertebrate embryos. *PLoS One*, *4*, e5887.

Werneburg, I., Laurin, M., Koyabu, D., & Sánchez-Villagra, M. (2016). Evolution of organogenesis and the origin of altriciality in mammals. *Evolution and Development*, *18*, 229–244.

Werneburg, I., Maier, W., & Joyce, W. G. (2013). Embryonic remnants of intercentra and cervical ribs in turtles. *Biology Open*, *2*, 1103–1107.

Werneburg, I., Polachowski, K., & Hutchinson, M. (2015). Bony skull development in the Argus monitor (Squamata, Varanidae, *Varanus panoptes*) with comments on developmental timing and adult anatomy. *Zoology*, *118*, 255–280.

Werneburg, I., & Sánchez-Villagra, M. R. (2009). Timing of organogenesis support basal position of turtles in the amniote tree of life. *BMC Evolutionary Biology*, *9*, 82. doi:10.1186/1471-2148-9-82

Yaryhin, O., & Werneburg, I. (2017). Chondrification and character identification in the skull exemplified for the basicranial anatomy of early squamate embryos. *Journal of Experimental Zoology*, *328B*, 476–488.

Yaryhin, O., & Werneburg, I. (2018). Tracing the developmental origin of a lizard skull: Chondrocranial architecture, heterochrony, and variation in lacertids. *Journal of Morphology*, *279*, 1058–1087.

SUPPORTING INFORMATION

Additional supporting information may be found in the online version of the article at the publisher's website.

How to cite this article: Schlindwein, X., Yaryhin, O., & Werneburg, I. (2022). Discrete embryonic character variation uncovers hidden ecological adaptations in lacertid lizards. *Development, Growth & Differentiation*, *64*(3), 178–191. https://doi.org/10.1111/dgd.12777

Supplemantary Tables

Table S1. SES data for all *Darevskia armeniaca* embryos, scaled by maximum incubation time (compare chapter 4.2)

specimen	DA81	DA61	DA49	DA59	DA82	DA51	DA74	DA47	DA73	DA57	DA77	DA72
egg lay date		28-29.06.2015	24.06.15	28-29.06.2015		28-29.06.2015	09.07.11	21.06.15	28-29.06.2015	24.06.15	07.07.11	28-29.06.2015
date of fixation	21.06.12	04.07.15	04.07.15	08.07.15	24.06.12	09.07.15	21.07.11	04.07.15	12.07.15	09.07.15	22.07.11	14.07.15
days incubated	2	7	11	11	11	12	13	14	15	16	16	17
fixation												
place												
C4. Posterior neuropore closed	0.03030303	0.106060606	0.166666667	0.166666667	0.166666667	0.181818182	0.196969697	0.212121212	0.227272727	0.242424242	0.242424242	0.257575758
D1. Somites hard to count		0.106060606	0.166666667	0.166666667	0.166666667	0.181818182	0.196969697	0.212121212	0.227272727	0.242424242	0.242424242	0.257575758
E2. Anterior cephalic projection	0.03030303	0.106060606	0.166666667	0.166666667	0.166666667	0.181818182	0.196969697	0.212121212	0.227272727	0.242424242	0.242424242	0.257575758
E3. Head projection disappeared												
F1. Olfactory placode	0.03030303											
F2. External nares		0.106060606	0.166666667	0.166666667	0.166666667	0.181818182	0.196969697	0.212121212	0.227272727		0.242424242	
F3. Nostrils formed												
G1. Otic placode	0.03030303	0.106060606			0.166666667							
G2. Otic vesicle							0.196969697		0.227272727	0.242424242	0.242424242	0.257575758
G3. Otic capsule inconspicuous												
H2. Lens placode	0.03030303	0.106060606			0.166666667							
H3. Optic fissure	0.03030303		0.166666667	0.166666667	0.166666667	0.181818182	0.196969697	0.212121212	0.227272727			
H4. Contour lens/iris						0.181818182	0.196969697		0.227272727		0.242424242	0.257575758
H5. Pupil forms										0.242424242		0.257575758
H7. Scleral papillae inconspicuous												
J1. Ventricle bulbus	0.03030303	0.106060606	0.166666667	0.166666667	0.166666667	0.181818182	0.196969697	0.212121212	0.227272727		0.242424242	0.257575758
J2. Thoracal bulbus disappeared												
J3. Ventricle S-shaped	0.03030303		0.166666667	0.166666667	0.166666667	0.181818182	0.196969697	0.212121212				
L1. Forelimb ridge	0.03030303											
L3. Forelimb bud		0.106060606			0.166666667							
L5. Forelimb elongated			0.166666667	0.166666667								
L7. Forelimb AER		0.106060606	0.166666667	0.166666667								
L9. Forelimb elbow						0.181818182	0.196969697		0.227272727	0.242424242	0.242424242	0.257575758
L11. Forelimb paddle												
L13. Forelimb digital plate						0.181818182	0.196969697		0.227272727			
L15. Digital grooves forelimb												
L17. Digital serration forelimb										0.242424242	0.242424242	0.257575758
L19. Finger										0.242424242		
L21. First claw forelimb												
25. Membranes between the fingers are completely gone.												
L27. Separate phalanges are visible in the fingers.												
L2. Hind limb ridge												
L4. Hind limb bud		0.106060606	0.166666667	0.166666667	0.166666667							
L6. Hind limb elongated								0.212121212				
L8. Hindlimb AER				0.166666667				0.212121212				
L10. Hind limb knee						0.181818182	0.196969697		0.227272727	0.242424242	0.242424242	0.257575758
L12. Hind limb paddle												
L14. Hind limb digital plate						0.181818182	0.196969697		0.227272727			
L16. Digital grooves hind limb												
L18. Digital serration hind limb										0.242424242	0.242424242	0.257575758
L20. Toe										0.242424242		
L22. First claw hind limb												
L26. Membranes between the toes are completely gone.												
L28. Separate phalanges are visible in the toes.												
M1. Head scales												
M2. Throat scales												
M3. Lower eyelid scales												
M4. Neck scales												
M5. Back scales												
M6. Forelimb scales proximal												
M7. Forelimb scales distal												
M8. Hind limb scales proximal												
M9. Hind limb scales distal												
M10. Tail scales												
O1. Maxillary bud												
O2. Maxillary process posterior to eye	0.03030303	0.106060606										
O3. Maxillary process midline of eye												
O4. Maxillary process anterior to lens			0.166666667	0.166666667								
O5. Maxillary process anterior to eye						0.181818182	0.196969697		0.227272727		0.242424242	
O6. Maxillary process fuses with frontonasal process										0.242424242		0.257575758
P1. Mandibular arch bud	0.03030303	0.106060606										
P2. process of the mandibular arch posterior eye			0.166666667	0.166666667				0.212121212				
P3. Mandibular arch bud posterior lens						0.181818182						
P4. Mandibular arch bud midline eye							0.196969697		0.227272727			
P5. Mandibular arch bud anterior lens												
P6. Mandibular arch bud anterior eye											0.242424242	
P7. Mandibular arch bud level frontonasal groove												0.257575758
P8. Mandibular arch bud occlusion point = jaw closure										0.242424242		
Q1. Second arch bud												
Q2. Hyoid flap			0.166666667	0.166666667		0.181818182						
Q3. Third arch bud												
Q4. Fourth arch bud	0.03030303											
Q5. Fifth arch bud		0.106060606			0.166666667							
R1. First pharyngeal slit												
R2. Second pharyngeal slit												
R3. Third pharyngeal slit	0.03030303		0.166666667									
R4. Fourth pharyngeal slit		0.106060606			0.166666667							
R5. Pharyngeal slits closed											0.242424242	
T1. Cervical flexure 90°	0.03030303	0.106060606	0.166666667	0.166666667	0.166666667	0.181818182	0.196969697			0.242424242		0.257575758
T2. Cervical flexure disappeared											0.242424242	
T4. Nuchal fold	0.03030303	0.106060606	0.166666667	0.166666667	0.166666667							
U1. Lower lid appears												
U2. Eyelid begun overgrow							0.196969697		0.227272727	0.242424242		0.257575758
U3. Eyelid at level of scleral papillae												
U4. Eyelid ventral to lens												
U5. Eyelid covers eye (at least half of it)												

specimen	DA55	DA21	DA24	DA64	DA22	DA50	DA52	DA70	DA46	DA7	DA67	DA26
egg lay date	19-20.06.2015	04.07.11	28-29.06.2015	21.06.15	04.07.11	19.06.15	21.06.15	28-29.06.2015	19-20.06.2015	28.06.11	19-20.06.2015	28-29.06.2015
date of fixation	04.07.15	22.07.11	16.07.15	10.07.15	24.07.11	10.07.15	12.07.15	19.07.15	13.07.15	22.07.11	14.07.15	23.07.15
days incubated	18	19	19	20	21	22	22	22	24	25	25	26
fixation		F			F					F		
place		UDZ	UDZ		UDZ					UDZ		UDZ
C4. Posterior neuropore closed	0.272727273	0.287878788	0.287878788	0.303030303	0.318181818	0.333333333	0.333333333	0.333333333	0.363636364	0.378787879	0.378787879	0.393939394
D1. Somites hard to count	0.272727273	0.287878788	0.287878788	0.303030303	0.318181818	0.333333333	0.333333333	0.333333333	0.363636364	0.378787879	0.378787879	0.393939394
E2. Anterior cephalic projection	0.272727273	0.287878788	0.287878788	0.303030303	0.318181818	0.333333333	0.333333333	0.333333333	0.363636364	0.378787879	0.378787879	0.393939394
E3. Head projection disappeared												
F1. Olfactory placode												
F2. External nares		0.287878788			0.318181818				0.363636364			
F3. Nostrils formed												
G1. Otic placode												
G2. Otic vesicle		0.287878788	0.287878788		0.318181818	0.333333333	0.333333333	0.333333333	0.363636364	0.378787879	0.378787879	0.393939394
G3. Otic capsule inconspicuous												
H2. Lens placode												
H3. Optic fissure	0.272727273	0.287878788			0.318181818							
H4. Contour lens/iris	0.272727273	0.287878788	0.287878788	0.303030303	0.318181818		0.333333333	0.333333333	0.363636364	0.378787879		0.393939394
H5. Pupil forms			0.287878788	0.303030303			0.333333333	0.333333333	0.363636364		0.378787879	0.393939394
H7. Scleral papillae inconspicuous												
J1. Ventricle bulbus	0.272727273	0.287878788	0.287878788	0.303030303	0.318181818				0.363636364	0.378787879		
J2. Thoracal bulbus disappeared						0.333333333	0.333333333				0.378787879	0.393939394
J3. Ventricle S-shaped	0.272727273											
L1. Forelimb ridge												
L3. Forelimb bud												
L5. Forelimb elongated												
L7. Forelimb AER												
L9. Forelimb elbow	0.272727273	0.287878788		0.303030303	0.318181818		0.333333333	0.333333333	0.363636364	0.378787879	0.378787879	0.393939394
L11. Forelimb paddle												
L13. Forelimb digital plate	0.272727273											
L15. Digital grooves forelimb												
L17. Digital serration forelimb		0.287878788			0.318181818				0.363636364			
L19. Finger			0.287878788	0.303030303		0.333333333	0.333333333	0.333333333		0.378787879		0.393939394
L21. First claw forelimb												
25. Membranes between the fingers are completely gone.												
L27. Separate phalanges are visible in the fingers.											0.378787879	
L2. Hind limb ridge												
L4. Hind limb bud												
L6. Hind limb elongated												
L8. Hindlimb AER												
L10. Hind limb knee	0.272727273	0.287878788	0.287878788	0.303030303	0.318181818	0.333333333	0.333333333	0.333333333	0.363636364	0.378787879	0.378787879	0.393939394
L12. Hind limb paddle												
L14. Hind limb digital plate	0.272727273											
L16. Digital grooves hind limb												
L18. Digital serration hind limb		0.287878788			0.318181818				0.363636364			
L20. Toe			0.287878788	0.303030303		0.333333333	0.333333333	0.333333333		0.378787879		0.393939394
L22. First claw hind limb												
L26. Membranes between the toes are completely gone.												
L28. Separate phalanges are visible in the toes.											0.378787879	
M1. Head scales												
M2. Throat scales												
M3. Lower eyelid scales												
M4. Neck scales												
M5. Back scales												
M6. Forelimb scales proximal												
M7. Forelimb scales distal												
M8. Hind limb scales proximal												
M9. Hind limb scales distal												
M10. Tail scales												
O1. Maxillary bud												
O2. Maxillary process posterior to eye												
O3. Maxillary process midline of eye												
O4. Maxillary process anterior to lens												
O5. Maxillary process anterior to eye		0.287878788			0.318181818							
O6. Maxillary process fuses with frontonasal process	0.272727273			0.303030303		0.333333333	0.333333333	0.333333333	0.363636364	0.378787879	0.378787879	0.393939394
P1. Mandibular arch bud												
P2. process of the mandibular arch posterior eye												
P3. Mandibular arch bud posterior lens												
P4. Mandibular arch bud midline eye												
P5. Mandibular arch bud anterior lens	0.272727273	0.287878788										
P6. Mandibular arch bud anterior eye					0.318181818							
P7. Mandibular arch bud level frontonasal groove				0.303030303					0.363636364			
P8. Mandibular arch bud occlusion point = jaw closure						0.333333333	0.333333333	0.333333333		0.378787879	0.378787879	0.393939394
Q1. Second arch bud												
Q2. Hyoid flap												
Q3. Third arch bud												
Q4. Fourth arch bud												
Q5. Fifth arch bud												
R1. First pharyngeal slit												
R2. Second pharyngeal slit												
R3. Third pharyngeal slit												
R4. Fourth pharyngeal slit												
R5. Pharyngeal slits closed		0.287878788	0.287878788	0.303030303	0.318181818	0.333333333	0.333333333	0.333333333	0.363636364	0.378787879	0.378787879	0.393939394
T1. Cervical flexure 90°	0.272727273	0.287878788	0.287878788	0.303030303	0.318181818		0.333333333	0.333333333	0.363636364		0.378787879	0.393939394
T2. Cervical flexure disappeared						0.333333333				0.378787879		
T4. Nuchal fold												
U1. Lower lid appears												
U2. Eyelid begun overgrow				0.303030303		0.333333333	0.333333333	0.333333333				0.393939394
U3. Eyelid at level of scleral papillae											0.378787879	
U4. Eyelid ventral to lens												
U5. Eyelid covers eye (at least half of it)												

specimen	DA40	DA80	DA36	DA5	DA11	DA9	DA12	DA13	DA15	DA16	DA17	DA76
egg lay date	21.06.15	22.06.11	22.06.15	23.06.11	28.06.11	28.06.11	28.06.11	28.06.11	28.06.11	28.06.11	28.06.11	28.06.11
date of fixation	16.07.15	22.07.11	23.07.15	27.07.11	03.08.11	05.08.11	05.08.11	07.08.11	15.08.11	17.08.11	19.08.11	26.08.11
days incubated	26	31	32	35	37	39	39	41	49	51	53	60
fixation				F	F	F	F	F	F	F	F	
place	UDZ		UDZ	UDZ	UDZ	UDZ	UDZ	UDZ	UDZ	UDZ	UDZ	
C4. Posterior neuropore closed	0.393939394	0.46969697	0.484848485	0.53030303	0.560606061	0.590909091	0.590909091	0.621212121	0.742424242	0.772727273	0.803030303	0.909090909
D1. Somites hard to count	0.393939394	0.46969697	0.484848485	0.53030303	0.560606061	0.590909091	0.590909091	0.621212121	0.742424242	0.772727273	0.803030303	0.909090909
E2. Anterior cephalic projection	0.393939394	0.46969697		0.53030303								
E3. Head projection disappeared								0.621212121	0.742424242	0.772727273	0.803030303	0.909090909
F1. Olfactory placode												
F2. External nares		0.46969697		0.53030303								
F3. Nostrils formed									0.742424242	0.772727273	0.803030303	0.909090909
G1. Otic placode												
G2. Otic vesicle	0.393939394	0.46969697		0.53030303								
G3. Otic capsule inconspicuous					0.560606061	0.590909091	0.590909091	0.621212121	0.742424242	0.772727273	0.803030303	0.909090909
H2. Lens placode												
H3. Optic fissure		0.46969697		0.53030303								
H4. Contour lens/iris	0.393939394	0.46969697										
H5. Pupil forms	0.393939394											
H7. Scleral papillae inconspicuous			0.484848485		0.560606061	0.590909091	0.590909091	0.621212121	0.742424242	0.772727273	0.803030303	0.909090909
J1. Ventricle bulbus		0.46969697		0.53030303								
J2. Thoracal bulbus disappeared	0.393939394		0.484848485		0.560606061	0.590909091	0.590909091	0.621212121	0.742424242	0.772727273	0.803030303	0.909090909
J3. Ventricle S-shaped				0.53030303								
L1. Forelimb ridge												
L3. Forelimb bud												
L5. Forelimb elongated												
L7. Forelimb AER												
L9. Forelimb elbow	0.393939394	0.46969697	0.484848485		0.560606061	0.590909091	0.590909091	0.621212121	0.742424242	0.772727273	0.803030303	0.909090909
L11. Forelimb paddle												
L13. Forelimb digital plate												
L15. Digital grooves forelimb		0.46969697										
L17. Digital serration forelimb												
L19. Finger												
L21. First claw forelimb			0.484848485		0.560606061	0.590909091	0.590909091	0.621212121	0.742424242	0.772727273	0.803030303	0.909090909
25. Membranes between the fingers are completely gone.			0.484848485		0.560606061	0.590909091	0.590909091	0.621212121	0.742424242	0.772727273	0.803030303	0.909090909
L27. Separate phalanges are visible in the fingers.	0.393939394		0.484848485		0.560606061	0.590909091	0.590909091	0.621212121	0.742424242	0.772727273	0.803030303	0.909090909
L2. Hind limb ridge												
L4. Hind limb bud												
L6. Hind limb elongated												
L8. Hindlimb AER												
L10. Hind limb knee	0.393939394	0.46969697	0.484848485		0.560606061	0.590909091	0.590909091	0.621212121	0.742424242	0.772727273	0.803030303	0.909090909
L12. Hind limb paddle												
L14. Hind limb digital plate												
L16. Digital grooves hind limb		0.46969697										
L18. Digital serration hind limb												
L20. Toe												
L22. First claw hind limb			0.484848485		0.560606061	0.590909091	0.590909091	0.621212121	0.742424242	0.772727273	0.803030303	0.909090909
L26. Membranes between the toes are completely gone.			0.484848485		0.560606061	0.590909091	0.590909091	0.621212121	0.742424242	0.772727273	0.803030303	0.909090909
L28. Separate phalanges are visible in the toes.	0.393939394		0.484848485		0.560606061	0.590909091	0.590909091	0.621212121	0.742424242	0.772727273	0.803030303	0.909090909
M1. Head scales									0.742424242	0.772727273	0.803030303	0.909090909
M2. Throat scales			0.484848485		0.560606061	0.590909091	0.590909091	0.621212121	0.742424242	0.772727273	0.803030303	0.909090909
M3. Lower eyelid scales											0.803030303	0.909090909
M4. Neck scales			0.484848485		0.560606061	0.590909091	0.590909091	0.621212121	0.742424242	0.772727273	0.803030303	0.909090909
M5. Back scales			0.484848485		0.560606061	0.590909091	0.590909091	0.621212121	0.742424242	0.772727273	0.803030303	0.909090909
M6. Forelimb scales proximal			0.484848485		0.560606061	0.590909091	0.590909091	0.621212121	0.742424242	0.772727273	0.803030303	0.909090909
M7. Forelimb scales distal						0.590909091		0.621212121	0.742424242	0.772727273	0.803030303	0.909090909
M8. Hind limb scales proximal			0.484848485		0.560606061	0.590909091	0.590909091	0.621212121	0.742424242	0.772727273	0.803030303	0.909090909
M9. Hind limb scales distal									0.742424242	0.772727273	0.803030303	0.909090909
M10. Tail scales			0.484848485		0.560606061	0.590909091	0.590909091	0.621212121	0.742424242	0.772727273	0.803030303	0.909090909
O1. Maxillary bud												
O2. Maxillary process posterior to eye												
O3. Maxillary process midline of eye												
O4. Maxillary process anterior to lens				0.53030303								
O5. Maxillary process anterior to eye												
O6. Maxillary process fuses with frontonasal process	0.393939394		0.484848485		0.560606061	0.590909091	0.590909091	0.621212121	0.742424242	0.772727273	0.803030303	0.909090909
P1. Mandibular arch bud												
P2. process of the mandibular arch posterior eye												
P3. Mandibular arch bud posterior lens				0.53030303								
P4. Mandibular arch bud midline eye												
P5. Mandibular arch bud anterior lens												
P6. Mandibular arch bud anterior eye												
P7. Mandibular arch bud level frontonasal groove												
P8. Mandibular arch bud occlusion point = jaw closure	0.393939394		0.484848485		0.560606061	0.590909091	0.590909091	0.621212121	0.742424242	0.772727273	0.803030303	0.909090909
Q1. Second arch bud												
Q2. Hyoid flap				0.53030303								
Q3. Third arch bud												
Q4. Fourth arch bud				0.53030303								
Q5. Fifth arch bud												
R1. First pharyngeal slit												
R2. Second pharyngeal slit												
R3. Third pharyngeal slit												
R4. Fourth pharyngeal slit				0.53030303								
R5. Pharyngeal slits closed	0.393939394		0.484848485		0.560606061	0.590909091	0.590909091	0.621212121	0.742424242	0.772727273	0.803030303	0.909090909
T1. Cervical flexure 90°	0.393939394			0.53030303								
T2. Cervical flexure disappeared			0.484848485		0.560606061	0.590909091	0.590909091	0.621212121	0.742424242	0.772727273	0.803030303	0.909090909
T4. Nuchal fold				0.53030303								
U1. Lower lid appears												
U2. Eyelid begun overgrow												
U3. Eyelid at level of scleral papillae	0.393939394											
U4. Eyelid ventral to lens			0.484848485		0.560606061	0.590909091	0.590909091					
U5. Eyelid covers eye (at least half of it)								0.621212121	0.742424242		0.803030303	0.909090909

Table S2. SES data for all *Lacerta viridis* embryos, scaled by maximum incubation time (compare chapter 4.2)

specimen	LV16	LV13	LV15	LV8	LV10	LV9	LV7	LV12	LV11	LV5	LV1	LV3	LV4	LV2	LV6
egg lay date	25.05.07	25.05.07	25.05.07	27.05.07	27.05.07	27.05.07	27.05.07	27.05.07	27.05.07	27.05.07	27.05.07	27.05.07	27.05.07	27.05.07	27.05.07
date of fixation	07.06.07	09.06.07	13.06.07	23.06.07	01.07.07	05.07.07	09.07.07	11.07.07	13.07.07	17.07.07	23.07.07	25.07.07	01.08.07	04.08.07	19.08.07
days incubated	14	16	20	31	36	40	44	46	48	52	58	60	67	70	85
fixation	F	F	F	F	F	F	F	F	F	F	F	F	F	F	F
place	UDE	UDE	UDE	UDE	UDE	UDE	UDE	UDE	UDE	UDE	UDE	UDE	UDE	UDE	UDE
C4. Posterior neuropore closed	0.155555556	0.177777778	0.222222222	0.344444444	0.4	0.444444444	0.488888889	0.511111111	0.533333333	0.577777778	0.644444444	0.666666667	0.744444444	0.777777778	0.944444444
D1. Somites hard to count	0.155555556	0.177777778	0.222222222	0.344444444	0.4	0.444444444	0.488888889	0.511111111	0.533333333	0.577777778	0.644444444	0.666666667	0.744444444	0.777777778	0.944444444
E2. Anterior cephalic projection	0.155555556	0.177777778	0.222222222	0.344444444	0.4	0.444444444	0.488888889	0.511111111	0.533333333	0.577777778	0.644444444	0.666666667	0.744444444	0.777777778	
E3. Head projection disappeared															
F1. Olfactory placode															
F2. External nares	0.155555556	0.177777778	0.222222222	0.344444444											
F3. Nostrils formed												0.666666667	0.744444444	0.777777778	0.944444444
G1. Otic placode															
G2. Otic vesicle	0.155555556	0.177777778	0.222222222	0.344444444		0.444444444									
G3. Otic capsule inconspicuous					0.4		0.488888889	0.511111111	0.533333333				0.744444444	0.777777778	0.944444444
H2. Lens placode															
H3. Optic fissure	0.155555556	0.177777778	0.222222222	0.344444444	0.4	0.444444444									
H4. Contour lens/iris				0.344444444	0.4	0.444444444	0.488888889	0.511111111	0.533333333	0.577777778		0.666666667			
H5. Pupil forms							0.488888889	0.511111111	0.533333333	0.577777778		0.666666667			
H7. Scleral papillae inconspicuous											0.644444444		0.744444444	0.777777778	0.944444444
J1. Ventricle bulbus	0.155555556	0.177777778	0.222222222	0.344444444											
J2. Thoracal bulbus disappeared					0.4		0.488888889	0.511111111	0.533333333				0.744444444	0.777777778	0.944444444
J3. Ventricle S-shaped	0.155555556		0.222222222												
L1. Forelimb ridge															
L3. Forelimb bud															
L5. Forelimb elongated															
L7. Forelimb AER															
L9. Forelimb elbow	0.155555556	0.177777778	0.222222222												
L11. Forelimb paddle	0.155555556														
L13. Forelimb digital plate			0.222222222	0.344444444											
L15. Digital grooves forelimb															
L17. Digital serration forelimb					0.4										
L19. Finger						0.444444444	0.488888889	0.511111111	0.533333333	0.577777778		0.666666667			
L21. First claw forelimb											0.644444444		0.744444444	0.777777778	0.944444444
25. Membranes between the fingers are completely gone.													0.744444444	0.777777778	0.944444444
L27. Separate phalanges are visible in the fingers.											0.644444444		0.744444444	0.777777778	0.944444444
L2. Hind limb ridge															
L4. Hind limb bud	0.155555556														
L6. Hind limb elongated		0.177777778													
L8. Hindlimb AER		0.177777778													
L10. Hind limb knee															
L12. Hind limb paddle			0.222222222												
L14. Hind limb digital plate															
L16. Digital grooves hind limb				0.344444444											
L18. Digital serration hind limb					0.4										
L20. Toe						0.444444444	0.488888889	0.511111111	0.533333333	0.577777778	0.644444444	0.666666667			
L22. First claw hind limb													0.744444444	0.777777778	0.944444444
L26. Membranes between the toes are completely gone.											0.644444444		0.744444444		0.944444444
L28. Separate phalanges are visible in the toes.													0.744444444	0.777777778	0.944444444
M1. Head scales													0.744444444		
M2. Throat scales													0.744444444	0.777777778	
M3. Lower eyelid scales															
M4. Neck scales											0.644444444		0.744444444	0.777777778	
M5. Back scales											0.644444444		0.744444444	0.777777778	
M6. Forelimb scales proximal											0.644444444		0.744444444	0.777777778	
M7. Forelimb scales distal													0.744444444	0.777777778	
M8. Hind limb scales proximal											0.644444444		0.744444444	0.777777778	
M9. Hind limb scales distal													0.744444444	0.777777778	
M10. Tail scales											0.644444444		0.744444444	0.777777778	
O1. Maxillary bud															
O2. Maxillary process posterior to eye															
O3. Maxillary process midline of eye	0.155555556														
O4. Maxillary process anterior to lens															
O5. Maxillary process anterior to eye		0.177777778	0.222222222	0.344444444											
O6. Maxillary process fuses with frontonasal process					0.4	0.444444444	0.488888889	0.511111111	0.533333333	0.577777778		0.666666667	0.744444444		0.944444444
P1. Mandibular arch bud	0.155555556														
P2. process of the mandibular arch posterior eye															
P3. Mandibular arch bud posterior lens		0.177777778	0.222222222												
P4. Mandibular arch bud midline eye															
P5. Mandibular arch bud anterior lens				0.344444444											
P6. Mandibular arch bud anterior eye															
P7. Mandibular arch bud level frontonasal groove															
P8. Mandibular arch bud occlusion point = jaw closure					0.4	0.444444444	0.488888889	0.511111111	0.533333333	0.577777778	0.644444444	0.666666667	0.744444444	0.777777778	0.944444444
Q1. Second arch bud															
Q2. Hyoid flap		0.177777778	0.222222222												
Q3. Third arch bud															
Q4. Fourth arch bud															
Q5. Fifth arch bud	0.155555556	0.177777778													
R1. First pharyngeal slit															
R2. Second pharyngeal slit															
R3. Third pharyngeal slit															
R4. Fourth pharyngeal slit	0.155555556	0.177777778													
R5. Pharyngeal slits closed					0.4	0.444444444	0.488888889	0.511111111	0.533333333	0.577777778	0.644444444	0.666666667	0.744444444	0.777777778	0.944444444
T1. Cervical flexure 90°	0.155555556	0.177777778	0.222222222												
T2. Cervical flexure disappeared				0.344444444		0.444444444	0.488888889	0.511111111	0.533333333	0.577777778		0.666666667	0.744444444	0.777777778	0.944444444
T4. Nuchal fold	0.155555556	0.177777778	0.222222222												
U1. Lower lid appears															
U2. Eyelid begun overgrow					0.4	0.444444444	0.488888889	0.511111111	0.533333333			0.666666667			
U3. Eyelid at level of scleral papillae															
U4. Eyelid ventral to lens											0.644444444			0.777777778	0.944444444
U5. Eyelid covers eye (at least half of it)													0.744444444		

Table S3. SES data for all *Lacerta agilis* embryos, scaled by maximum incubation time (compare chapter 4.2)

specimen	LA26	LA31	LA16	LA17	LA18	LA19	LA20	LA24	LA21	LA25	LA27	LA33	LA36	LA37	LA10	LA11	LA12
egg lay date	21.06.07	30.05.07	27.06.07	27.06.07	27.06.07	27.06.07	27.06.07	23.06.07	27.06.07	23.06.07	21.06.07	14.06.07	24.06.08	13.06.08	13.05.13	13.05.13	13.05.13
date of fixation	21.06.07	01.06.07	29.06.07	01.07.07	02.07.07	03.07.07	04.07.07	30.06.07	05.07.07	01.07.07	30.06.07	21.06.07	04.07.08	01.07.08	11.06.13	13.06.13	16.06.13
days incubated	1	2	3	5	6	7	8	8	9	9	10	11	11	19	30	32	35
fixation	F	F	F	F	F	F	F	F	F	F	F	F	F	F	F	F	F
place	UZM	UKT	UZM	UZM	UZM	UZM	UZM	UZM	UZM	UZM	UZM	UZM	UZM	UZM	UKC	UKC	UKC
C4. Posterior neuropore closed	0.015384615	0.030769231	0.046153846	0.076923077	0.092307692	0.107692308	0.123076923	0.123076923	0.138461538	0.138461538	0.153846154	0.169230769	0.169230769	0.292307692	0.461538462	0.492307692	0.538461538
D1. Somites hard to count	0.015384615	0.030769231	0.046153846	0.076923077	0.092307692	0.107692308	0.123076923	0.123076923	0.138461538	0.138461538	0.153846154	0.169230769	0.169230769	0.292307692	0.461538462	0.492307692	0.538461538
E2. Anterior cephalic projection	0.015384615	0.030769231	0.046153846	0.076923077	0.092307692	0.107692308	0.123076923	0.123076923	0.138461538	0.138461538	0.153846154	0.169230769	0.169230769	0.292307692	0.461538462	0.492307692	0.538461538
E3. Head projection disappeared																	
F1. Olfactory placode	0.015384615	0.030769231	0.046153846	0.076923077	0.092307692												
F2. External nares							0.123076923	0.123076923	0.138461538	0.138461538	0.153846154	0.169230769	0.169230769	0.292307692	0.461538462	0.492307692	
F3.Nostrils formed																	
G1. Otic placode	0.015384615	0.030769231	0.046153846	0.076923077	0.092307692	0.107692308	0.123076923	0.123076923	0.138461538	0.138461538							
G2. Otic vesicle											0.153846154	0.169230769	0.169230769	0.292307692	0.461538462	0.492307692	0.538461538
G3. Otic capsule inconspicuous																	
H2. Lens placode	0.015384615		0.046153846		0.092307692	0.107692308	0.123076923										
H3. Optic fissure		0.030769231		0.076923077				0.123076923	0.138461538	0.138461538	0.153846154	0.169230769	0.169230769		0.461538462	0.492307692	0.538461538
H4. Contour lens/iris														0.292307692	0.461538462	0.492307692	0.538461538
H5. Pupil forms																	0.538461538
H7. Scleral papillae inconspicuous																	
J1. Ventricle bulbus	0.015384615	0.030769231	0.046153846	0.076923077	0.092307692	0.107692308	0.123076923	0.123076923	0.138461538	0.138461538	0.153846154	0.169230769	0.169230769		0.461538462	0.492307692	
J2. Thoracal bulbus disappeared																	0.538461538
J3. Ventricle S-shaped	0.015384615	0.030769231	0.046153846	0.076923077	0.092307692	0.107692308	0.123076923	0.123076923	0.138461538	0.138461538	0.153846154						
L1. Forelimb ridge		0.030769231															
L3. Forelimb bud	0.015384615		0.046153846	0.076923077			0.123076923										
L5. Forelimb elongated						0.107692308			0.138461538	0.138461538	0.153846154	0.169230769					
L7. Forelimb AER						0.107692308	0.123076923		0.138461538	0.138461538	0.153846154	0.169230769					
L8. Forelimb elbow													0.169230769	0.292307692	0.461538462	0.492307692	0.538461538
L11. Forelimb paddle													0.169230769				
L13.Forelimb digital plate																	
L15. Digital grooves forelimb														0.292307692	0.461538462		
L17. Digital serration forelimb																0.492307692	
L19. Finger																	0.538461538
L21. First claw forelimb																	
L25. Membranes between the fingers are completely gone.																	
L27. Separate phalanges are visible in the fingers.																	
L2. Hind limb ridge	0.015384615	0.030769231	0.046153846														
L4. Hind limb bud						0.107692308	0.123076923	0.123076923	0.138461538	0.138461538	0.153846154	0.169230769					
L6. Hind limb elongated																	
L8. Hindlimb AER						0.107692308	0.123076923	0.123076923	0.138461538	0.138461538	0.153846154	0.169230769					
L10. Hind limb knee														0.292307692	0.461538462	0.492307692	0.538461538
L12. Hind limb paddle													0.169230769				
L14. Hind limb digital plate																	
L16. Digital grooves hind limb														0.292307692	0.461538462		
L18. Digital serration hind limb																0.492307692	
L20. Toe																	0.538461538
L22. First claw hind limb																	
L26. Membranes between the toes are completely gone.																	
L28. Separate phalanges are visible in the toes.																	
M1. Head scales																	
M2. Throat scales																	
M3. Lower eyelid scales																	
M4. Neck scales																	
M5. Back scales																	
M6. Forelimb scales proximal																	
M7. Forelimb scales distal																	
M8. Hind limb scales proximal																	
M9. Hind limb scales distal																	
M10. Tail scales																	
O1. Maxillary bud	0.015384615	0.030769231	0.046153846	0.076923077													
O2. Maxillary process posterior to eye					0.092307692	0.107692308											
O3. Maxillary process midline of eye							0.123076923	0.123076923									
O4. Maxillary process anterior to lens									0.138461538	0.138461538	0.153846154	0.169230769					
O5. Maxillary process anterior to eye													0.169230769		0.461538462		
O6. Maxillary process fuses with frontonasal process														0.292307692		0.492307692	0.538461538
P1. Mandibular arch bud	0.015384615	0.030769231	0.046153846	0.076923077													
P2. process of the mandibular arch posterior eye					0.092307692	0.107692308											
P3. Mandibular arch bud posterior lens							0.123076923	0.123076923	0.138461538	0.138461538	0.153846154	0.169230769	0.169230769				
P4. Mandibular arch bud midline eye															0.461538462		
P5. Mandibular arch bud anterior lens																	
P6. Mandibular arch bud anterior eye																	
P7. Mandibular arch bud level frontonasal groove														0.292307692		0.492307692	
P8. Mandibular arch bud occlusion point = jaw closure																	0.538461538
Q1. Second arch bud																	
Q2. Hyoid flap										0.138461538	0.153846154		0.169230769				
Q3. Third arch bud																	
Q4. Fourth arch bud		0.030769231	0.046153846	0.076923077	0.092307692	0.107692308											
Q5. Fifth arch bud							0.123076923	0.123076923	0.138461538		0.153846154	0.169230769					
R1. First pharyngeal slit																	
R2. Second pharyngeal slit																	
R3. Third pharyngeal slit		0.030769231															
R4. Fourth pharyngeal slit			0.046153846	0.076923077	0.092307692	0.107692308	0.123076923	0.123076923	0.138461538		0.153846154	0.169230769					
R5. Pharyngeal slits closed														0.292307692			
T1. Cervical flexure 90°	0.015384615	0.030769231	0.046153846	0.076923077	0.092307692	0.107692308	0.123076923	0.123076923	0.138461538	0.138461538	0.153846154	0.169230769	0.169230769	0.292307692	0.461538462	0.492307692	0.538461538
T2. Cervical flexure disappeared																	
T4. Nuchal fold		0.030769231	0.046153846	0.076923077	0.092307692	0.107692308		0.123076923	0.138461538	0.138461538	0.153846154	0.169230769					
U1. Lower lid appears																	
U2. Eyelid begun overgrow														0.292307692	0.461538462		0.538461538
U3. Eyelid at level of scleral papillae																	
U4. Eyelid ventral to lens																	
U5. Eyelid covers eye (at least half of it)																	

specimen	LA01	LA39	LA40	LA13	LA29	LA09	LA14	LA34	LA03	LA02	LA38	LA15	LA06	LA04	LA08	LA05
egg lay date	31.05.07	13-14.05.2013	13-14.05.2014	13.05.13	01.07.07	23.06.07	13.05.13	16.06.08		31.05.07	13.06.08	13.05.13	23.06.07	21.06.07	23.06.07	
date of fixation	05.07.07	20.06.13	22.06.14	25.06.13	13.08.07	06.08.07	27.06.13	31.07.08		13.07.07	31.07.08	01.07.13	17.08.07	19.08.07	23.08.07	
days incubated	36	39	41	44	44	45	46	46	47	48	49	50	56	60	62	63
fixation	F			F	F	F	F	F	F	F	F	F	F	F	F	F
place	UKT	UKC	UKC	UKC	UZM	UZM	UKC	UKT	UKT	UKT		UKC	UZM	UZM	UZM	UZM
C4. Posterior neuropore closed	0.553846154	0.6	0.630769231	0.676923077	0.676923077	0.692307692	0.707692308	0.707692308	0.723076923	0.738461538	0.753846154	0.769230769	0.861538462	0.923076923	0.953846154	0.969230769
D1. Somites hard to count	0.553846154	0.6	0.630769231	0.676923077	0.676923077	0.692307692	0.707692308	0.707692308	0.723076923	0.738461538	0.753846154	0.769230769	0.861538462	0.923076923	0.953846154	0.969230769
E2. Anterior cephalic projection	0.553846154	0.6	0.630769231	0.676923077		0.692307692	0.707692308		0.723076923	0.738461538						
E3. Head projection disappeared					0.676923077			0.707692308			0.753846154	0.769230769	0.861538462	0.923076923	0.953846154	0.969230769
F1. Olfactory placode																
F2. External nares																
F3. Nostrils formed		0.6	0.630769231	0.676923077	0.676923077	0.692307692	0.707692308	0.707692308	0.723076923	0.738461538	0.753846154	0.769230769	0.861538462	0.923076923	0.953846154	0.969230769
G1. Otic placode																
G2. Otic vesicle																
G3. Otic capsule inconspicuous		0.6	0.630769231	0.676923077	0.676923077	0.692307692	0.707692308	0.707692308	0.723076923	0.738461538	0.753846154	0.769230769	0.861538462	0.923076923	0.953846154	0.969230769
H2. Lens placode																
H3. Optic fissure																
H4. Contour lens/iris																
H5. Pupil forms	0.553846154	0.6	0.630769231			0.692307692			0.723076923	0.738461538						
H7. Scleral papillae inconspicuous				0.676923077	0.676923077		0.707692308	0.707692308			0.753846154	0.769230769	0.861538462	0.923076923	0.953846154	0.969230769
J1. Ventricle bulbus																
J2. Thoracal bulbus disappeared	0.553846154	0.6	0.630769231	0.676923077	0.676923077	0.692307692	0.707692308	0.707692308	0.723076923	0.738461538	0.753846154	0.769230769	0.861538462	0.923076923	0.953846154	0.969230769
J3. Ventricle S-shaped																
L1. Forelimb ridge																
L3. Forelimb bud																
L5. Forelimb elongated																
L7. Forelimb AER																
L8. Forelimb elbow	0.553846154	0.6	0.630769231	0.676923077	0.676923077	0.692307692	0.707692308	0.707692308	0.723076923	0.738461538	0.753846154	0.769230769	0.861538462	0.923076923	0.953846154	0.969230769
L11. Forelimb paddle																
L13.Forelimb digital plate																
L15. Digital grooves forelimb																
L17. Digital serration forelimb																
L19. Finger	0.553846154	0.6	0.630769231	0.676923077	0.676923077	0.692307692	0.707692308	0.707692308	0.723076923	0.738461538	0.753846154	0.769230769	0.861538462	0.923076923	0.953846154	0.969230769
L21. First claw forelimb	0.553846154		0.630769231	0.676923077	0.676923077	0.692307692	0.707692308	0.707692308	0.723076923	0.738461538	0.753846154	0.769230769	0.861538462	0.923076923	0.953846154	0.969230769
L25. Membranes between the fingers are completely gone.			0.630769231	0.676923077	0.676923077	0.692307692	0.707692308	0.707692308	0.723076923	0.738461538	0.753846154	0.769230769	0.861538462	0.923076923	0.953846154	0.969230769
L27. Separate phalanges are visible in the fingers.	0.553846154		0.630769231	0.676923077	0.676923077	0.692307692	0.707692308	0.707692308	0.723076923	0.738461538	0.753846154	0.769230769	0.861538462	0.923076923	0.953846154	0.969230769
L2. Hind limb ridge																
L4. Hind limb bud																
L6. Hind limb elongated																
L8. Hindlimb AER																
L10. Hind limb knee	0.553846154	0.6	0.630769231	0.676923077	0.676923077	0.692307692	0.707692308	0.707692308	0.723076923	0.738461538	0.753846154	0.769230769	0.861538462	0.923076923	0.953846154	0.969230769
L12. Hind limb paddle																
L14. Hind limb digital plate																
L16. Digital grooves hind limb																
L18. Digital serration hind limb																
L20. Toe	0.553846154	0.6	0.630769231	0.676923077	0.676923077	0.692307692	0.707692308	0.707692308	0.723076923	0.738461538	0.753846154	0.769230769	0.861538462	0.923076923	0.953846154	0.969230769
L22. First claw hind limb				0.676923077	0.676923077	0.692307692	0.707692308	0.707692308			0.753846154	0.769230769	0.861538462	0.923076923	0.953846154	0.969230769
L26. Membranes between the toes are completely gone.				0.676923077	0.676923077	0.692307692	0.707692308	0.707692308	0.723076923	0.738461538	0.753846154	0.769230769	0.861538462	0.923076923	0.953846154	0.969230769
L28. Separate phalanges are visible in the toes.	0.553846154		0.630769231	0.676923077	0.676923077	0.692307692	0.707692308	0.707692308	0.723076923	0.738461538	0.753846154	0.769230769	0.861538462	0.923076923	0.953846154	0.969230769
M1. Head scales											0.753846154	0.769230769	0.861538462	0.923076923	0.953846154	0.969230769
M2. Throat scales				0.676923077	0.676923077	0.692307692	0.707692308		0.723076923	0.738461538	0.753846154	0.769230769	0.861538462	0.923076923	0.953846154	0.969230769
M3. Lower eyelid scales														0.923076923	0.953846154	0.969230769
M4. Neck scales			0.630769231	0.676923077	0.676923077	0.692307692	0.707692308	0.707692308	0.723076923	0.738461538	0.753846154	0.769230769	0.861538462	0.923076923	0.953846154	0.969230769
M5. Back scales			0.630769231	0.676923077	0.676923077	0.692307692	0.707692308	0.707692308	0.723076923	0.738461538	0.753846154	0.769230769	0.861538462	0.923076923	0.953846154	0.969230769
M6. Forelimb scales proximal				0.676923077	0.676923077		0.707692308	0.707692308	0.723076923	0.738461538	0.753846154	0.769230769	0.861538462	0.923076923	0.953846154	0.969230769
M7. Forelimb scales distal							0.707692308	0.707692308	0.723076923	0.738461538	0.753846154	0.769230769	0.861538462	0.923076923	0.953846154	0.969230769
M8. Hind limb scales proximal				0.676923077	0.676923077		0.707692308	0.707692308	0.723076923	0.738461538	0.753846154	0.769230769	0.861538462	0.923076923	0.953846154	0.969230769
M9. Hind limb scales distal											0.753846154	0.769230769	0.861538462	0.923076923	0.953846154	0.969230769
M10. Tail scales				0.676923077	0.676923077	0.692307692	0.707692308	0.707692308	0.723076923	0.738461538	0.753846154	0.769230769	0.861538462	0.923076923	0.953846154	0.969230769
O1. Maxillary bud																
O2. Maxillary process posterior to eye																
O3. Maxillary process midline of eye																
O4. Maxillary process anterior to lens																
O5. Maxillary process anterior to eye																
O6. Maxillary process fuses with frontonasal process	0.553846154	0.6	0.630769231	0.676923077	0.676923077	0.692307692	0.707692308	0.707692308	0.723076923	0.738461538	0.753846154	0.769230769	0.861538462	0.923076923	0.953846154	0.969230769
P1. Mandibular arch bud																
P2. process of the mandibular arch posterior eye																
P3. Mandibular arch bud posterior lens																
P4. Mandibular arch bud midline eye																
P5. Mandibular arch bud anterior lens																
P6. Mandibular arch bud anterior eye																
P7. Mandibular arch bud level frontonasal groove																
P8. Mandibular arch bud occlusion point = jaw closure	0.553846154	0.6	0.630769231	0.676923077	0.676923077	0.692307692	0.707692308	0.707692308	0.723076923	0.738461538	0.753846154	0.769230769	0.861538462	0.923076923	0.953846154	0.969230769
Q1. Second arch bud																
Q2. Hyoid flap																
Q3. Third arch bud																
Q4. Fourth arch bud																
Q5. Fifth arch bud																
R1. First pharyngeal slit																
R2. Second pharyngeal slit																
R3. Third pharyngeal slit																
R4. Fourth pharyngeal slit																
R5. Pharyngeal slits closed	0.553846154	0.6	0.630769231	0.676923077	0.676923077	0.692307692	0.707692308	0.707692308	0.723076923	0.738461538	0.753846154	0.769230769	0.861538462	0.923076923	0.953846154	0.969230769
T1. Cervical flexure 90°	0.553846154	0.6														
T2. Cervical flexure disappeared			0.630769231	0.676923077	0.676923077	0.692307692	0.707692308	0.707692308	0.723076923	0.738461538	0.753846154	0.769230769	0.861538462	0.923076923	0.953846154	0.969230769
T4. Nuchal fold																
U1. Lower lid appears																
U2. Eyelid begun overgrow		0.6	0.630769231													
U3. Eyelid at level of scleral papillae	0.553846154					0.692307692										
U4. Eyelid ventral to lens				0.676923077			0.707692308		0.723076923							

Table S4. Earliest, latest, and mean occurrence of SES data for all species, including outgroup and reconstructed, ancestral sequence

	Darevskia armeniaca			*Lacerta viridis*			*Lacerta agilis*			*Salvator merianae*	Lacerta	Lacertidae
	early	mean	late	early	mean	late	early	mean	late			
C3. Anterior neuropore closed										0.05		
C4. Posterior neuropore closed	0.03030303	0.37920875	0.90909091	0.15555556	0.50888889	0.94444444	0.01538462	0.96923077	0.45780886	0.05	0.46039176	0.41151531
D1. Somites hard to count	0.10606061	0.38917749	0.90909091	0.15555556	0.50888889	0.94444444	0.01538462	0.96923077	0.45780886	0.083333333	0.46240872	0.41782645
D5. 16-20 somite pairs										0.05		
D6. 21-25 somite pairs										0.066666667		
E1. Head bulbus										0.05		
E2. Anterior cephalic projection	0.03030303	0.28058361	0.53030303	0.15555556	0.47777778	0.77777778	0.01538462	0.73846154	0.33969231	0.05	0.38435271	0.33244193
E3. Head projection disappeared	0.62121212	0.76969697	0.90909091				0.67692308	0.96923077	0.82692308	0.3		0.75867173
F1. Olfactory placode	0.03030303	0.03030303	0.03030303				0.01538462	0.09230769	0.05230769	0.066666667		0.04332274
F2. External nares	0.10606061	0.25974026	0.53030303	0.15555556	0.225	0.34444444	0.12307692	0.49230769	0.22615385	0.166666667	0.22865189	0.2351986
F3. Nostrils formed	0.74242424	0.80681818	0.90909091	0.66666667	0.78333333	0.94444444	0.6	0.96923077	0.75897436	0.25	0.764177	0.74932306
G1. Otic placode	0.03030303	0.1010101	0.16666667				0.01538462	0.13846154	0.08923077	0.05		0.09153131
G2. Otic vesicle	0.1969697	0.33164983	0.53030303	0.15555556	0.26888889	0.44444444	0.15384615	0.53846154	0.32527473	0.066666667	0.29640776	0.29497269
G3. Otic capsule inconspicuous	0.56060606	0.69886364	0.90909091	0.4	0.62857143	0.94444444	0.6	0.96923077	0.75897436	0.233333333	0.68422135	0.6638858
H2. Lens placode	0.03030303	0.1010101	0.16666667				0.01538462	0.12307692	0.07692308	0.05		0.08586697
H3. Optic fissure	0.03030303	0.24825175	0.53030303	0.15555556	0.29074074	0.44444444	0.03076923	0.53846154	0.22657343	0.066666667	0.25306797	0.24116856
H4. Contour lens/iris	0.18181818	0.3083779	0.46969697	0.34444444	0.49583333	0.66666667	0.29230769	0.53846154	0.44615385	0.1	0.44192045	0.38002281
H5. Pupil forms	0.24242424	0.32878788	0.39393939	0.48888889	0.55555556	0.66666667	0.53846154	0.73846154	0.63956044	0.166666667	0.55354592	0.45984277
H7. Scleral papillae inconspicuous	0.48484848	0.67508418	0.90909091	0.64444444	0.77777778	0.94444444	0.67692308	0.96923077	0.8		0.77320913	0.73982641
J1. Ventricle bulbus	0.03030303	0.25833333	0.53030303	0.15555556	0.225	0.34444444	0.01538462	0.49230769	0.15589744	0.05	0.19604048	0.20794553
J2. Thoracal bulbus disappeared	0.33333333	0.56493506	0.90909091	0.4	0.62857143	0.94444444	0.53846154	0.96923077	0.73393665	0.35	0.65899794	0.61161399
J3. Ventricle S-shaped	0.03030303	0.21380471	0.53030303	0.15555556	0.18888889	0.22222222	0.01538462	0.15384615	0.0951049		0.15189041	0.17295404
L01. Forelimb ridge	0.03030303	0.03030303	0.03030303				0.03076923	0.03076923	0.03076923	0.066666667		0.03341015
L02. Hind limb ridge							0.01538462	0.04615385	0.03076923	0.066666667		
L03. Forelimb bud	0.10606061	0.13636364	0.16666667				0.01538462	0.12307692	0.06538462	0.083333333		0.09947884
L04. Hind limb bud	0.10606061	0.15151515	0.16666667	0.15555556	0.15555556	0.15555556	0.10769231	0.16923077	0.13626374	0.083333333	0.14524158	0.14381925
L05. Forelimb elongated	0.16666667	0.16666667	0.16666667				0.10769231	0.16923077	0.14153846	0.1		0.14979895
L06. Hind limb elongated	0.21212121	0.21212121	0.21212121	0.17777778	0.17777778	0.17777778				0.1		0.18739669
L07. Forelimb AER	0.10606061	0.14646465	0.16666667				0.10769231	0.16923077	0.13846154	0.116666667		0.1404111
L08. Hindlimb AER	0.16666667	0.18939394	0.21212121	0.17777778	0.17777778	0.17777778	0.10769231	0.16923077	0.13626374	0.116666667	0.16027743	0.16721099
L09. Forelimb elbow	0.18181818	0.4315376	0.90909091	0.15555556	0.18518519	0.22222222	0.16923077	0.96923077	0.66153846	0.183333333	0.41909062	0.40999709
L10. Hind limb knee	0.18181818	0.42319749	0.90909091				0.29230769	0.96923077	0.68615385	0.183333333		0.52513707
L11. Forelimb paddle				0.15555556	0.15555556	0.15555556	0.16923077	0.16923077	0.16923077		0.16239316	
L12. Hind limb paddle				0.22222222	0.22222222	0.22222222	0.16923077	0.16923077	0.16923077		0.1957265	
L13. Forelimb digital plate	0.18181818	0.21969697	0.27272727	0.22222222	0.28333333	0.34444444				0.166666667		0.24476584
L14. Hind limb digital plate	0.18181818	0.21969697	0.27272727							0.166666667		
L15. Digital grooves forelimb	0.46969697	0.46969697	0.46969697				0.29230769	0.46153846	0.37692308	0.183333333		0.40422097
L16. Digital grooves hind limb	0.46969697	0.46969697	0.46969697	0.34444444	0.34444444	0.34444444	0.29230769	0.46153846	0.37692308	0.233333333	0.37183946	0.39559031
L17. Digital serration forelimb	0.24242424	0.28535354	0.36363636	0.4	0.4	0.4	0.49230769	0.49230769	0.49230769	0.25	0.4211883	0.36803584
L18. Digital serration hind limb	0.24242424	0.28535354	0.36363636	0.4	0.4	0.4	0.49230769	0.49230769	0.49230769	0.25		0.37778727
L19. Finger	0.24242424	0.32575758	0.39393939	0.44444444	0.53703704	0.66666667	0.53846154	0.96923077	0.73393665	0.3	0.5883372	0.48795409
L20. Toe	0.24242424	0.32575758	0.39393939	0.44444444	0.55238095	0.66666667	0.53846154	0.96923077	0.73393665	0.3	0.59485541	0.49201592
L21. First claw forelimb	0.48484848	0.67508418	0.90909091	0.64444444	0.77777778	0.94444444	0.55384615	0.96923077	0.75589744	0.4	0.74694278	0.70458605
L22. First claw hind limb	0.48484848	0.67508418	0.90909091	0.74444444	0.82222222	0.94444444	0.67692308	0.96923077	0.79020979	0.35	0.77929113	0.72196721
L25. Membranes between the fingers are completely gone.	0.48484848	0.67508418	0.90909091	0.74444444	0.82222222	0.94444444	0.63076923	0.96923077	0.77032967	0.45	0.77306212	0.72363914
L26. Membranes between the toes are completely gone.	0.48484848	0.67508418	0.90909091	0.64444444	0.77777778	0.94444444	0.67692308	0.96923077	0.78106509	0.4	0.75763418	0.71124842
L27. Separate phalanges are visible in the fingers.	0.37878788	0.62258953	0.90909091	0.64444444	0.77777778	0.94444444	0.55384615	0.96923077	0.75589744	0.4	0.74021174	0.6835244
L28. Separate phalanges are visible in the toes.	0.37878788	0.62258953	0.90909091	0.74444444	0.82222222	0.94444444	0.55384615	0.96923077	0.75589744	0.4	0.75909206	0.6952897
M01. Head scales	0.74242424	0.80681818	0.90909091	0.74444444	0.74444444	0.74444444	0.75384615	0.96923077	0.87179487	0.45	0.8000161	0.78276337
M02. Throat scales	0.48484848	0.67508418	0.90909091	0.74444444	0.76111111	0.77777778	0.67692308	0.96923077	0.78717949	0.5	0.75536771	0.71538961
M03. Lower eyelid scales	0.8030303	0.85606061	0.90909091				0.92307692	0.96923077	0.94871795	0.6		0.87833558
M04. Neck scales	0.48484848	0.67508418	0.90909091	0.64444444	0.72222222	0.77777778	0.63076923	0.96923077	0.77032967	0.6	0.73390571	0.70756908
M05. Back scales	0.48484848	0.67508418	0.90909091	0.64444444	0.72222222	0.77777778	0.63076923	0.96923077	0.77032967	0.35	0.72836519	0.69023262
M06. Forelimb scales proximal	0.48484848	0.67508418	0.90909091	0.64444444	0.72222222	0.77777778	0.67692308	0.96923077	0.78846154	0.45	0.73828395	0.70196706
M07. Forelimb scales distal	0.59090909	0.73989899	0.90909091	0.74444444	0.76111111	0.77777778	0.70769231	0.96923077	0.81076923	0.5	0.77369958	0.74763898
M08. Hind limb scales proximal	0.48484848	0.67508418	0.90909091	0.64444444	0.72222222	0.77777778	0.67692308	0.96923077	0.78846154	0.45	0.73828395	0.70196706
M09. Hind limb scales distal	0.74242424	0.80681818	0.90909091	0.74444444	0.76111111	0.77777778	0.75384615	0.96923077	0.87179487	0.5	0.80820433	0.79064265
M10. Tail scales	0.48484848	0.67508418	0.90909091	0.64444444	0.72222222	0.77777778	0.67692308	0.96923077	0.78106509	0.35	0.73292568	0.69307449
O1. Maxillary bud							0.01538462	0.07692308	0.04230769	0.066666667		
O2. Maxillary process posterior to eye	0.03030303	0.06818182	0.10606061				0.09230769	0.10769231	0.1	0.083333333		0.08403065
O3. Maxillary process midline of eye				0.15555556	0.15555556	0.15555556	0.12307692	0.12307692	0.12307692		0.19318553	0.30787499
O4. Maxillary process anterior to lens	0.16666667	0.28787879	0.53030303				0.13846154	0.16923077	0.15	0.116666667		0.15501894
O5. Maxillary process anterior to eye	0.18181818	0.24242424	0.31818182	0.17777778	0.24814815	0.34444444	0.16923077	0.46153846	0.31538462	0.166666667	0.27417095	0.25800002
O6. Maxillary process fuses with frontonasal process	0.24242424	0.47907648	0.90909091	0.4	0.59012346	0.94444444	0.29230769	0.96923077	0.69797571	0.183333333	0.61268573	0.54591108
P1. Mandibular arch bud	0.03030303	0.06818182	0.10606061	0.15555556	0.15555556	0.15555556	0.01538462	0.07692308	0.04230769	0.066666667	0.11402531	0.14616026
P2. process of the mandibular arch posterior eye	0.16666667	0.18181818	0.21212121				0.09230769	0.10769231	0.1	0.166666667		0.14295799
P3. Mandibular arch bud posterior lens	0.18181818	0.35606061	0.53030303	0.17777778	0.2	0.22222222	0.12307692	0.16923077	0.14505495	0.183333333	0.17395824	0.17700439
P4. Mandibular arch bud midline eye	0.1969697	0.21212121	0.22727273				0.46153846	0.46153846	0.46153846			0.33682984
P5. Mandibular arch bud anterior lens	0.27272727	0.28030303	0.28787879	0.34444444	0.34444444	0.34444444						0.31237374
P6. Mandibular arch bud anterior eye	0.24242424	0.28030303	0.31818182							0.233333333		
P7. Mandibular arch bud level frontonasal groove	0.25757576	0.30808081	0.36363636				0.29230769	0.49230769	0.39230769	0.25		0.34222425
P8. Mandibular arch bud occlusion point = jaw closure	0.24242424	0.52139037	0.90909091	0.4	0.61212121	0.94444444	0.53846154	0.96923077	0.73393665	0.35	0.64642632	0.5897885
Q1. Second arch bud												
Q2. Hyoid flap	0.16666667	0.26136364	0.53030303	0.17777778	0.2	0.22222222	0.13846154	0.16923077	0.15384615	0.166666667	0.18752303	0.21009068
Q3. Third arch bud										0.05		
Q4. Fourth arch bud	0.03030303	0.28030303	0.53030303				0.03076923	0.10769231	0.07076923	0.066666667		0.16687606
Q5. Fifth arch bud	0.10606061	0.13636364	0.16666667	0.15555556	0.16666667	0.17777778	0.12307692	0.16923077	0.14153846	0.1	0.15062899	0.14323365
R3. Third pharyngeal slit	0.03030303	0.09848485	0.16666667				0.03076923	0.03076923	0.03076923	0.05		0.06346352
R4. Fourth pharyngeal slit	0.10606061	0.26767677	0.53030303	0.15555556	0.16666667	0.17777778	0.04615385	0.16923077	0.11452991	0.1	0.15599299	0.1887688
R5. Pharyngeal slits closed	0.24242424	0.4738292	0.90909091	0.4	0.61212121	0.94444444	0.29230769	0.96923077	0.70940171	0.183333333	0.62621156	0.55265371
T1. Cervical flexure 90°	0.03030303	0.27200577	0.53030303	0.15555556	0.18518519	0.22222222	0.01538462	0.6	0.22753036	0.05	0.21131017	0.22185399
T2. Cervical flexure disappeared	0.24242424	0.58585859	0.90909091	0.34444444	0.60333333	0.94444444	0.63076923	0.96923077	0.77032967	0.3	0.67251418	
T4. Nuchal fold	0.03030303	0.19444444	0.53030303	0.15555556	0.18518519	0.22222222	0.03076923	0.16923077	0.10769231		0.15305286	0.16713454
U2. Eyelid begun overgrow	0.1969697	0.29124579	0.39393939	0.4	0.50740741	0.66666667	0.29230769	0.63076923	0.50461538	0.35	0.47501587	0.4090254
U3. Eyelid at level of scleral papillae	0.37878788	0.38636364	0.39393939				0.55384615	0.69230769	0.62307692	0.4		0.49639026
U4. Eyelid ventral to lens	0.48484848	0.55681818	0.59090909	0.64444444	0.78888889	0.94444444	0.67692308	0.72307692	0.7025641	0.55	0.71716631	0.65636076
U5. Eyelid covers eye (at least half of it)	0.62121212	0.76893939	0.90909091	0.74444444	0.74444444	0.74444444	0.67692308	0.96923077	0.82692308	0.6	0.7794216	0.76608926